Last Interglacial sea surface warming during the sea-level highstand in the Canary Islands: Implications for the Canary Current and the upwelling off African coast

Chloé Maréchal, Antoine Boutier, Marie-Antoinette Mélières, Thibault Clauzel, Juan Francisco Betancort, Alejandro Lomoschitz, Joaquin Meco, François Fourel, Abel Barral, Romain Amiot, et al.

Last Interglacial sea surface warming during the sea-level highstand in the Canary Islands : Implications for the Canary Current and the upwelling off African coast

Chloé Maréchal[1,*], Antoine Boutier[2], Marie-Antoinette Mélières[3], Thibault Clauzel[4], Juan Francisco Betancort[5], Alejandro Lomoschitz[6], Joaquin Meco[5], François Fourel[7], Abel Barral[4], Romain Amiot[4], Christophe Lécuyer[4]

[1] Observatoire des Sciences de l'Univers de Lyon, Université Claude Bernard Lyon 1, France

[2] Dipartimento Scienze della Terra, Università degli Studi di Torino, Via Valperga Caluso 35, 10125 Torino, Italy

[3] African Patterns, Scientist committee, 23 Rue St Sulpice, 75006 Paris, France

[4] Laboratoire de Géologie de Lyon, CNRS UMR 5276, Université Claude Bernard Lyon 1, France

[5] Departamento de Biología, Universidad de Las Palmas de Gran Canaria, ULPGC, 35017 Las Palmas de Gran Canaria, Canary Islands, Spain

[6] Instituto de Oceanografía y Cambio Global, IOCAG – Unidad Asociada de I+D+i al CSIC, Universidad de Las Palmas de Gran Canaria, ULPGC, 35017 Las Palmas de Gran Canaria, Canary Islands, Spain

[7] Laboratoire d'Ecologie des Hydrosystèmes Naturels et Anthropisés, CNRS UMR 5023, Université Claude Bernard Lyon 1, France

Keywords : LIG; MIS5e; Sea-level; Sea surface temperature; Stable isotopes; Molluscs; Canary current; Upwelling; North Atlantic Gyre ; Climate change

Abstract – The Canary Islands, east of the North Atlantic Ocean (27°N-29°N), are under the influence of the Canary Current, the descending branch of the North Atlantic Gyre, which is modulated by coastal upwelling off North-West Africa. They constitute strategic sites for palaeoclimatic reconstructions, especially for the Last Interglacial (LIG, 129 to 116 ky BP) estimated to be warmer than present. Seventy-four carbon and oxygen isotope bulk analyses and time series measurements were performed on 32 aragonitic mollusc shells from the LIG marine deposits on Lanzarote and Fuerteventura islands during a period of sea-level highstand that we estimated to occur between ≈125 and 119-116 ky BP. Our SST calculations, inferred from shell $\delta^{18}O$ values using available isotopic fractionation equations, provide a seasonal SST amplitude ranging from 3.5°C to 6.0°C, in agreement with the modern seasonal amplitude, along with a mean SST comprised between 20.4±1.3°C and 22.2±1.2°C. With respect to the pre-industrial times, we deduce a positive SST anomaly in the range of +1.0±1.4°C to +2.8±1.3°C, consistent with the presence of the species *Persististrombus latus*, typical of warm SSTs. Although this finding does not match with the zonal negative anomaly of a reconstructed SST at low latitudes of the North Atlantic, it is nevertheless corroborated by other climate reconstructions in the northeastern tropical Atlantic region. We attribute this trend to an excess of summer insolation during the LIG which warmed the Canary Current, enhanced by a weakening of the North African upwelling. The entire North Atlantic Gyre was probably warmer during the LIG.

Abbreviations used:

LIG : Last Interglacial period; GMST : Global Mean Surface Temperature; SST : Sea Surface Temperature; SL : Sea-level.

1. Introduction

Since pre-industrial times (middle of the 19th century) the global mean surface temperature (GMST) has increased by about 1°C due to the emission of anthropogenic greenhouse gases (IPCC, 2013). As these emissions will continue during the 21th century, global warming of between +2°C and +5°C is projected by the end of the century (IPCC, 2013). In such scenarios of large climate change, simulations of global warming must be performed with the highest precision possible. The confidence in the future climate simulations by models is tested through the ability of the same models to simulate past climates correctly, particularly climates warmer than the present. This calls for the most precise description of such past warm periods. Even though the cause of past warming differs from that of the present (i.e., not due to the greenhouse effect), it is of paramount importance that the state of the world in a warmer climate be accurately simulated.

Such findings are obtained from reconstitutions of regional and local climates, in which the temperature remains one of the key parameters. In the reconstitutions three criteria should be kept in mind : (1) a warmer than present context, (2) a geographical region, which, as far as possible, is consistent with the globally relevant climate mechanisms, and (3) a chronological framework that possesses sufficiently high precision for the data from the proxies used by the models.

The present study focuses on the sea surface temperature reconstruction during the Last Interglacial (LIG) in the Canary Islands (northeast tropical Atlantic) (Figure 1) from marine sediment deposits (Figure 2). It satisfies the above criteria in the following way :

(1) During the Quaternary glacial/interglacial oscillations, it is known that two interglacials were warmer than the present interglacial : the Marine Isotope Stage MIS11c, from ≈245 to ≈235 thousand years before present (ka BP), and the Last Interglacial (LIG) which covers approximately the time interval between ≈129 and ≈116 ka BP (Masson Delmotte et al.,

2013; Capron et al., 2017a). The LIG, i.e. the most recent, gives rise to a more detailed reconstitution. Moreover, of the last five Quaternary climate cycles, it appears to be the warmest interglacial (Jouzel et al., 2007; Past Interglacials Working Group of PAGES, 2016) by about +2°C with respect to the present interglacial.

(2) Temperature reconstructions during the LIG have recently been the subject of intense interest. Whereas many publications focus on the polar and mid latitude regions, temperature data from the tropics, particularly seawater surface temperature (SST) data, are much scarcer. The Canary Islands, located in the tropical northeast Atlantic along the west African coast, are exposed mainly to the southward marine Canary Current, the descending branch of the North Atlantic Gyre, and are also influenced by the cold coastal upwelling current off North-West Africa (Arístegui et al., 2009). The northeast tropical Atlantic region is particularly important from the point of view of ocean circulation because the North Atlantic Gyre, an essential component of the global circulation, participates directly in the climate equilibrium of the planet. At present, few LIG data exist for this region and those that do exist appear to be contradictory, some suggesting warming and others cooling. Reconstruction of the SST in this region is therefore of major importance.

(3) Over the last decades, the geology, sedimentology and chronology of the Canary Islands have been thoroughly investigated, as well as the composition of faunal taxa found in the marine fossil deposits and in paleosols (Meco and Stearns, 1981 ; Meco et al., 2002 ; Zazo et al., 2002 ; Meco et al., 2006 ; Meco et al., 2011 ; Muhs et al., 2014 ; Montesinos et al., 2014 ; Meco et al., 2018). This rich source of information is relevant to establishing the chronology of the deposits under study.

In this investigation, we used the oxygen and carbon isotope compositions of carbonate shells dating of the LIG in order to estimate not only the SST, but also the magnitude of seasonal temperature variations and the seasonal activity of the coastal

upwelling. This method has not been applied in the region yet. In order to obtain qualitative indications of local warming/cooling of the SST, we also reconstituted the living environment of the faunal fossil record. These new data complement other SST results from the tropical northeast tropical Atlantic and afford a deeper understanding of regional ocean currents: the upwelling off the western African coast and the Canary Current.

2. Background

2.1. Geological setting

The Canary Islands comprise seven main volcanic islands and several islets. They are located in the Eastern Atlantic Ocean between 27°N and 30°N, forming a chain that extends about 450 km in latitude, with the easternmost point just over 100 km off the north-western African coast (Figure 1a). The islands have a complex geological history, with volcanic formations over 20 million years old (Carracedo et al., 2002), but they also include extensive sedimentary deposits (Meco and Stearns, 1981). As part of this study, two specific sites with sedimentary deposits were sampled in the easternmost Canary Islands, namely Fuerteventura and Lanzarote. While the eastern Canary Islands experienced some uplift during the last million years, discontinuous vertical movements with a reverse trend over the last hundreds of thousands of years have been observed (Zazo et al., 2002).

In the Canary Islands, the sedimentary deposits are related to the glacial–interglacial cycles and are characterized by a succession of four distinct climatic phases (Meco et al., 2011): (i) calcareous dune deposits, corresponding to a cold and arid glacial climate, (ii) paleosols, corresponding to a climate that became progressively warm and wet at the beginning of the interglacial period, (iii) marine sediments deposited during the sea-level

highstand of the interglacial period, and (iv) pedogenic calcretes, marking the return to the next glaciation. These different phases were identified in the Eastern Canary Islands for the MIS11.3 interglacial period as well as for the MIS10–MIS9.3, MIS6–MIS5.5 (LIG) (Figure 2a), MIS2–MIS1 (Holocene) glacial–interglacial oscillations. In the Canary Islands, the warm and wet climate of phase (ii) that generated paleosol deposits is considered to be contemporaneous with the wet phase in West Africa ("African Humid Period"). The latter, evaluated through many proxies in different areas of North Africa, stems from the maximum summer insolation in the tropics (Rossignol-Strick, 1985; deMenocal et al., 2000).

LIG marine deposits are found in the Eastern Canary Islands. In Lanzarote, these deposits have outcrops mainly at the localities of La Santa, Matagorda and Punta Penedo (Meco et al., 2006; Muhs et al., 2014), whereas in Fuerteventura they occur at the localities of Matas Blancas, Las Playitas and La Guirra (Meco et al., 2002; Zazo et al., 2002; Meco et al., 2006; Montesinos et al., 2014; Meco et al., 2018) (Figure 1b). LIG marine deposits also occur in the central island of the archipelago in Las Palmas, Gran Canaria (Meco et al., 2002). In the present work two LIG marine deposits were studied: La Santa (Lanzarote) and Matas Blancas (Fuerteventura). The La Santa site (29°06’48,43’’N, 13°38’57,50’’W), which is located along the northwest coast of Lanzarote, is composed of fossiliferous marine sands overlying Middle Pleistocene basaltic lava flows at ~8 m above the present mean sea-level (Muhs et al., 2014). This sandy deposit developed in a foreshore environment. The same layer crops out at the Punta Penedo site, a few kilometers northeast of La Santa and shows the most complete section in the area (Figure 2a). The Matas Blancas site (28°10'26,60"N, 14°11'46,91"W) is located along the eastern coast of the Jandia Isthmus, in Southern Fuerteventura. The marine sedimentary deposit consists of an extensive fossiliferous marine conglomerate at -2 m to +3 m above the present medium sea-level, identified as a marine terrace (Meco et al., 2002). It is composed of coarse basaltic fragments and fossils with a calcareous sandy matrix and

includes abundant specimens of *Persististrombus latus* (also named *Strombus bubonius*) (Figure 2b). It originally developed in a high energetic foreshore environment, forming part of a gravel berm or a beach of pebbles and sand. The deposit appears naturally cemented and can be considered as a beachrock.

2.2. Modern oceanic features

The eastern part of the North Atlantic Gyre is driven by the eastward Azores Current which partly feeds the Canary Current, a southward-flowing current along the Northwest African coast (Figures 3a and 1a). As it passes the Canary Islands archipelago, the current splits in two, with branches to the east and west of Lanzarote. The surface current is associated with a strong coastal upwelling regime along the north-west African coast, caused by the northeast trade winds (Figure 3b). Strengthening of the alongshore wind enhances upwelling and results in lower SST over the shelf (Figure 3b). In the latitude range 22°N to 30°N, where the Canary Islands are located, the coastal upwelling is permanent all year round, with the strongest activity occurring in summer and early fall (Pardo et al., 2011; Navarro-Pérez and Barton, 2001; Mittelstaedt, 1991).

The recent mean annual temperature of the eastern Canary Islands coastal waters has been estimated by different methods (Table 1). In the framework of this study we retain the combined satellite data and *in situ* SST datasets from the eastern Canary Islands, which give a sea surface temperature (SST) of 20.4°C from 2007 to 2017 (Meco et al., 2018). This finding is consistent with the other satellite measurements.

3. Materials

175 3.1. Sample collection

176

177 Thirty-two fossil marine mollusc shells belonging to 6 different species were collected
178 in the eastern Canary Islands. The largest number of fossils was collected at La Santa site
179 (Lanzarote) with 28 fossil mollusc shells belonging to 5 different species, whereas 4 fossil
180 mollusc shells belonging to two different species were collected at Matas Blancas site
181 (Fuerteventura). The fossils are either gastropods (*Cerithium vulgatum* Bruguière, 1792;
182 *Stramonita haemastoma* Linnaeus, 1767; *Luria lurida* Linnaeus, 1758; *Persististrombus latus*,
183 Gmelin 1791, usually refered to as *Strombus bubonius* Lamarck, 1822) or bivalves (*Loripes*
184 *lacteus* Linnaeus, 1758 – *nomen nudum* ; *Cardium edule* Linnaeus, 1758, also named
185 *Cerastoderma edule* Linnaeus, 1758) (Figure 4). Quite prevalent in the LIG sample deposits,
186 they are representative of the sites, gastropods being more frequent than bivalves. They all
187 lived in nearshore environments and shallow sea beds (Cuerda, 1987*;* Niclès, 1950; Rolán,
188 2011; Meco, 1977; Cosel von and Gofas, 2019; Cosel von and Gofas, 2019, respectively).

189 Among the 6 studied species, one lives in warm waters: *Persististrombus latus*
190 (*Strombus bubonius*). This gastropod is currently found on the western African coasts from
191 Dakar in Senegal to Angola, including the Cape Verde Islands. It belongs to the tropical
192 Guinean/Senegalese faunal province (Muhs et al., 2014). In the Canary Islands, it is present
193 only in the form of fossil species in the marine deposits of previous interglacials (LIG and
194 MIS11) (Meco, 1977; Meco et al., 2002; Meco et al., 2007; Muhs et al., 2014). *Luria lurida*
195 and *Stramonita haemastoma* live in an environment of warm to cooler waters : *Luria lurida*
196 currently lives on the North-western African coasts from Morocco to Angola (Rolan et al.,
197 2011), whereas *Stramonita haemastoma* currently lives on the western African coasts from
198 Morocco to Angola, including the Canary Islands (Rolán, 2011). Finally, *Cardium edule*,
199 *Loripes lacteus and Cerithium vulgatum* live in cooler marine waters. *Cardium edule*

(*Cerastoderma edule*) is present in the north-western Atlantic and in the north-eastern Atlantic, from Iceland and North Europe to Senegal, but rarely in the Canary Islands (Rolán, 2011; Nicklès, 1950). *Loripes lacteus* currently lives in the Eastern Atlantic from England and the North Sea to Senegal (Rolán, 2011; Nicklès, 1950). *Cerithium vulgatum* currently lives in the Atlantic from Portugal and Morocco to the Canary archipelago (Rolán, 2011). All the species except *Persististrombus latus* (*Strombus bubonius*), which at present lives far south of the Canary Islands, are now present at the latitude of the Canary archipelago in the eastern Atlantic (Figure 5).

The shells were directly sampled from the sedimentary marine beds at the sites where they outcrop, then labelled and put into plastic bags.

3.2. Age of the sampled deposits

The age of the marine deposits containing the mollusc shells has been estimated by three different approaches : the various LIG fossil datings in the eastern Canary archipelago, the sea-level history during interglacials, and the sedimentary successions during glacial-interglacial cycles in the Canary Islands.

U-series dating of two fragments of coral *Siderastraea radians*, Pallas 1766 coming from San Cristobal, Gran Canaria, and La Santa marine deposits, and which are ascribed to the LIG sea-level highstand, yields the ages 120.5±0.8 ka and 130.2±0.8 ka, respectively (Muhs et al., 2014). Five marine terraces cropping out in Lanzarote, which are considered to be contemporaneous with those of La Santa on the basis of stratigraphic arguments, provided U-series ages from the aragonitic shells of the gastropod *Patella* of 121±17 ka BP (n = 11) (Zazo et al., 2002). At the Matas Blancas site, the gastropods *Persististrombus latus* (*Strombus bubonius*) has yielded numerous radiometric ages based on the U/Th method,

namely 106±7 and 112±7 ka BP according to Meco et al. (1992); 104±2 and 178±4 ka BP (Zazo et al., 2002); 115, 125 and 135 ka BP (Bard, personal communication in Meco et al., 2002). Dating of several mollusc shells from six other contemporaneous sites in Fuerteventura give mean U/Th ages of 118±11 ka BP (n = 22) (Zazo et al., 2002). Taken altogether, these results indicate that the La Santa and Matas Blancas marine deposits can be attributed to the LIG. Finally, the numerous U/Th datings at LIG sites in Lanzarote and Fuerteventura from Zazo et al. (2002) exhibit a first order normal distribution, thereby confirming the validity of the mean ages, despite the large standard deviation. According to these data, the marine sediments, aged 121±17 ka BP on Lanzarote and 118±11 ka BP on Fuerteventura, were probably deposited during the second part of the LIG.

As the shells analyzed in the present study were sampled from a marine deposit, the average age of the analyzed molluscan assemblage therefore corresponds to the average age of the deposit. Sedimentation took place during a steady period of sea-level highstand when sedimentary particles and shells could accumulate over a period of time long enough to generate substantial sedimentary formation, i.e., at least a few thousand years. To understand the general context in which our samples were deposited, we first present here the different reconstructions of sea-level evolution during the LIG. In order to reconstruct past sea-levels, many studies have relied on the oxygen isotope compositions of foraminifera tests trapped in marine sediments (Shackleton et al., 1987; McManus et al., 1999; Shackleton et al., 2000; Waelbroeck et al, 2002; Lisiecki and Raymo, 2005; Rohling et al., 2009; Sosdian and Rosenthal, 2009; Elderfield et al., 2012; Rohling et al., 2014; Shakun et al., 2015). In successive reviews the issue of sea-level and its relative variations during the LIG has received much attention in the scientific community. Different chronologies, deduced from proxy reconstructions and synthesis compilations, of the sea-level highstand during the LIG were compiled in Table 2. It should be noted that the diversity of chronological methods used

to quantify paleo-sea-levels has sometimes led to substantial differences in the acquisition and appreciation of ages, a fact that may contribute to uncertainty in the chronology of sea-level changes. Dutton et al. (2015a) specified that sea-level during the LIG varied from +6 m to +9 m, with a peak occurring after 125 ka BP, probably between 122 and 119 ka BP. Capron et al. (2017a,b), on the basis of the work made by Dutton et al. (2015a), emphasized that most studies consider a two-phase sea-level change during the LIG, including a late event that peaked between 122 and 119 ka BP. We conclude from all these works that during the LIG the global sea-level rose by between +6 m and +9 m, with a maximum rise that very likely took place in the second part of the LIG, after ≈125 ka BP, and extended for a few thousand years until 119-116 ka BP. Secondly, the age estimation of the onset of sea-level highstand during the LIG is corroborated by the history of sea-level and that of global surface temperature during the last deglaciation and the Holocene. The timing of the changes in the global mean surface temperature can be documented by that of the evolution of the Antarctic temperature (see § 6.2.2) (Figure 6b,c). During the Holocene, the mean surface temperature has remained maximum and relatively steady since ≈12 ka BP (Marcott et al., 2013) (Figure 6b). From ≈18 ka to ≈7 ka BP, the sea-level has risen by more than 120 metres (Waelbroeck et al., 2002; Lambeck et al., 2014) (Figure 6d). Dutton et al. (2015a) note that at the beginning of the Holocene the global mean sea-level was still ≈60 m lower than today. The sea-level highstand has been steady only since ≈7 ka BP. The delay of about 5 ka between the establishment of the maximum of the mean temperature and the establishment of the maximum mean sea-level stemmed mainly from the melting dynamics of ice sheets from the northern hemisphere and Antarctica. It follows that a time lag of a few thousand years between the beginning of the LIG and the beginning of the global mean sea-level highstand during the LIG is consistent with the history of the Holocene global mean sea-level. Since during the LIG the mean surface temperature reached its maximum at ≈130 ka BP (Figure

6c), which marks the beginning of the interglacial stage, we infer that sea-level highstand began at ≈125 ka BP (Figure 6e). Therefore, based on the history of the last deglaciation and that of the Holocene it is very likely that the LIG marine deposits took place during the long time period of the sea-level highstand starting from ≈125 ka BP to 119-116 ky BP.

Finally, the chronology of the sea-level highstand during the LIG and the resulting estimate of the age of our samples is corroborated by the stratigraphic analysis performed by Meco et al. (2011) in the Canary Islands (see §2.1). The beginning of interglacials is characterized by a humid phase ("African Humid Period") with the development of a soil (labelled (ii)); as sea-levels rise, the soil is covered by seawater and marine sediments begin to form (labelled (iii)). During MIS1 or the Holocene, the two phases (ii) and (iii) are clearly identified: (ii) paleosols were mainly established between ≈10 ka and ≈8 ka BP, (iii) marine deposits between ≈5 ka and ≈1 ka BP, as dated from different samplings (Meco et al., 2011) (Figure 6a). The genesis of paleosols thus preceded that of marine sediments by a few thousand years. Such observations are consistent with the timing of the sapropel deposits in the Mediterranean (Rossignol-Strick, 1985) known to be correlated with the maximum intensity of the African wet phase between ≈10 ka and ≈8 ka BP (deMenocal et al., 2000; Lézine et al., 2011). As the sea-level has remained steady since ≈ 7 ka BP (Lambeck et al., 2014), the marine deposits are contemporaneous with the sea-level highstand. During the LIG, these two phases are well documented, the paleosol formation (ii) preceding the marine deposit (iii) (Figure 2a). Therefore, as pointed out by Meco et al. (2011), the stratigraphy of the paleosols and marine deposits indicate that the paleosol formation occurred during the first part of the LIG, and was followed by the sea-level highstand few thousand years after the beginning of the LIG, in the second part of the interglacial. It was during this sea-level highstand that the marine deposits were set down.

Finally, the three different approaches (deposit dating, the sea-level highstand history, and succession of paleosols and marine deposits) led to the same conclusion : the marine deposits from La Santa, Lanzarote, and Matas Blancas, Fuerteventura, date from the second part of the LIG, i.e. from ≈125 ka to ≈119-116 ka BP, at a time of sea-level highstand.

4. Methods

4.1. Analytical techniques

4.1.1. Raman spectroscopy and mineralogy of the sample shells

We used Raman spectroscopy in order to characterize the mineralogy of all the studied skeletal carbonates. The Raman Spectrometer X'plora, hosted by the Laboratoire de Géologie de Lyon at the University Claude Bernard Lyon 1, has been operated by using an objective x 1000, an optical network of 1800 lines per mm, a monochromatic laser (wavelength of 532 nm) filtered by 10% with ten acquisitions (15 s per acquisition) performed between 100 and 1600 cm^{-1}.

Aragonite was systematically identified from the low frequency part of the Raman spectra (Figure 7), and especially from the position and splitting of the symmetric bending mode which occurs as a doublet at 701-704 cm^{-1} according to Unvros et al. (1991) and Gillet et al. (1993). These analyses attest that the fossils shells studied consist of aragonite. It is known that the calcite to aragonite transition takes place at high pressure/high temperature (Gillet et al., 1987). As the mollusc shells precipitate at low pressure/low temperature, any polymorphism transformation from calcite to aragonite is *a priori* prevented during the shell growth. Thus the biogenic carbonates are considered to be originally aragonitic and the fossils

pristine. This is confirmed by Raman spectroscopy on the modern bivalve *Cerastoderma edule* (or *Cardium edule*) species which forms an entirely aragonitic shell (Füllenbach et al., 2015). Also, Cornu et a. (1993) acknowledged that the inorganic part of the modern gastropod *Persististrombus latus* (*Strombus bubonius*) is composed exclusively of aragonite. Those two species are studied in the present work. Therefore, the results obtained by Raman spectroscopy, which indicate that the shell carbonate of the fossil specimens is aragonitic, are considered to be a reliable indicator of isotopic signal (O and C) preservation.

4.1.2. Oxygen and carbon isotope analysis of aragonite mollusc shells

Stable carbon and oxygen isotope compositions were measured on a total of 32 mollusc shells of 6 species. Selected samples were cleaned with double-deionized water, then placed in an ultrasonic bath to remove any trace of sediment, and finally dried in a dry-oven. Two types of sampling were performed : (1) bulk sampling, which delivers an average signal over the entire life of the specimen, and (2) incremental sampling, which delivers discrete signals during the ontogenic evolution of the specimen, i.e., sampling of different periods of the shell growth (younger to older periods). (1) For bulk shells, the entire sample was crushed with a hammer in a steel mortar to obtain a coarse powder, which we reduced to a fine powder (50 to 100 μm particle size) with a pestle and agate mortar. The aliquot size was about 300 μg of $CaCO_3$. Each shell represents one bulk sample. 30 shells from La Santa and Matas Blancas sites were selected for the bulk sampling, including 4 gastropods and 2 bivalves species. (2) For incremental sampling of the shells, first, as the surface of the outer shell layer is most often easily altered, the outermost part of the shell was gently removed using a diamond micro-drill (Dremel™). Second, after cleaning the shell with double-deionized water, the layer underneath the outermost surface of the shell was drilled at regular intervals along the

growth direction. Two shells from La Santa (Lanzarote) and Matas Blancas (Fuerteventura) sites were selected for the incremental sampling: one bivalve specimen and one gastropod specimen, respectively. For the bivalve *Cardium edule* (*Cerastoderma edule*), 16 incremental samplings were performed along its main growth axis, one sampling every ≈3 mm (Figure S1a,b in the Supplementary materials). As the average growth rate of the *Cardium edule* shells ranges from ≈1.8 mm.month^{-1} to ≈0.8 mm.month^{-1} (Richardson et al., 1980; Eisma et al., 1965), and as the growth rates decrease with increasing age (Bourget and Brock, 1990), we estimated that we performed one sampling every ≈2 to ≈4 months. For the gastropod *Stramonita haemastoma*, 29 incremental samplings were carried out, one sampling every ≈5 mm, the sampling scheme precisely following the growth spiral of the shell according to the protocol of Cornu et al. (1993) (Figure S1c,d).

Stable isotope ratios were determined by using an auto sampler MultiPrep™ system coupled to a dual–inlet GV Isoprime™ isotope ratio mass spectrometer (IRMS). For bulk shells, aliquot size was about 300 μg of calcium carbonate while they were about 10–15 μg in the case of an incremental sampling strategy. All aliquots were reacted with anhydrous oversaturated phosphoric acid at 90°C during 20 minutes. By default, oxygen isotope ratios of calcium carbonate are computed assuming an acid fractionation factor 1000lnα(CO_2–$CaCO_3$) of 8.1 between carbon dioxide and calcite according to Swart et al. (1991) experimental data. However, acid fractionation factors differ between aragonite and calcite as shown by Kim and O'Neil (1997) and Kim et al. (2007a). At a temperature of 90°C, the mean difference in acid fractionation factors between calcite and aragonite is -0.41‰ (Kim et al., 2007a). Consequently, such offset value was applied to all mollusc oxygen isotope measurements as all the samples are made of aragonite. In addition, all sample measurements were duplicated and adjusted to the international reference NIST NBS19 ($\delta^{18}O_{V\text{-}PDB}$ = -2.20‰; $\delta^{13}C_{V\text{-}PDB}$ = +1.95‰) and NIST NBS18 ($\delta^{18}O_{V\text{-}PDB}$ = -23.2‰; $\delta^{13}C_{V\text{-}PDB}$ = -5.01‰). External

reproducibility (2σ) is lower than ±0.10‰ for $\delta^{18}O$ and ±0.05‰ for $\delta^{13}C$. $\delta^{18}O$ and $\delta^{13}C$ of aragonite mollusc shells are expressed with respect to V-PDB.

4.2. Isotope fractionation equations for the aragonite-water system

The Raman spectra analyses indicate that the shell carbonate of the fossil specimens is aragonitic. As modern biogenic aragonites are precipitated close to oxygen isotope equilibrium with ambient water (Kim et al., 2007b), it is reasonable to assume that this condition was also met for past biogenic aragonites. Indeed, Grossman and Ku (1986) and Kim et al. (2007b) demonstrated that oxygen isotope fractionation between water and aragonite can be described by a well-constrained relationship with temperature, which is a necessary and sufficient condition for reconstructing marine paleotemperatures from aragonite fossils.

The sea surface temperatures were calculated using two oxygen isotope fractionation equations for the aragonite-water system. The first of these (Grossman and Ku, 1986) was determined by analyzing modern aragonitic molluscs, foraminifera and ambient water in the temperature range ≈ 3 to 22°C with $\delta^{18}O_{aragonite}$ ($\delta^{18}O_{ar}$) and $\delta^{18}O_{seawater}$ ($\delta^{18}O_{sw}$) relative to V-PDB:

$$T = 20.60 - 4.34(\delta^{18}O_{ar} - \delta^{18}O_{sw}) \quad (1)$$

where T (°C) is the temperature in which the shell grew. The second oxygen isotope fractionation equation (Kim et al., 2007b) was obtained from laboratory experiments with $\delta^{18}O_{ar}$ and $\delta^{18}O_{sw}$ relative to V-SMOW:

$$1000 \ln \alpha_{ar-sw} = 17.88\left(\frac{10^3}{T}\right) - 31.14 \quad (2)$$

T being the temperature in Kelvin, α the oxygen fractionation coefficient between synthetic aragonite and water:

$$\propto_{ar-sw} = \frac{\left(\frac{^{18}O}{^{16}O}\right)_{ar}}{\left(\frac{^{18}O}{^{16}O}\right)_{sw}} = \frac{\left(\delta^{18}O_{ar} + 1000\right)}{\left(\delta^{18}O_{sw} + 1000\right)} \quad (3)$$

As we need the $\delta^{18}O$ of the aragonitic shell expressed relative to the V-SMOW (Eq.(2)) we use the following relationship between the V-PDB isotope scale and the V-SMOW scale established at 25°C by Coplen et al. (1983):

$$\delta^{18}O_{(V\text{-}SMOW)} = 1.03091\delta^{18}O_{(V\text{-}PDB)} + 30.91 \quad (4)$$

The two temperature calibrations for the aragonite-water oxygen isotope fractionation have been tested on 50 modern shells, both gastropods and bivalves, in Crete, Greece, where present-day prevailing mean SSTs are similar to those of the Canary Islands (about 20°C) (Lécuyer et al., 2018). The SST calculated from the $\delta^{18}O$ values of those shells and $\delta^{18}O$ values of ambient seawater in Crete match the SST available from oceanic databases available for the Mediterranean Sea on using either the Kim et al. (2007b) equation or the Grossman and Ku (1986) equation. The best match between the present SST and calculated values was obtained by applying the Kim et al. (2007b) equation. Therefore it seems more appropriate to privilege the use of the Kim et al. (2007b) equation for calculating SST of Lanzarote and Fuerteventura coastal waters during the LIG. However, as Grossman and Ku (1986)'s

422 equation was established from an *in situ* calibration and is predominantly used in the literature
423 for SST reconstructions based on mollusc shells, we also present the results of this equation in
424 order to allow comparisons of the results of this study with other publications.
425
426 4.3. $\delta^{18}O$ reconstruction of coastal seawater during the LIG
427
428 Reconstitution of marine paleotemperatures based on the $\delta^{18}O$ values of aragonite
429 mollusc shells requires an estimate of the oxygen isotope composition of contemporaneous
430 seawater of the living shells (Equations (1) and (2)). In this study, we therefore estimated the
431 $\delta^{18}O$ of seawater during the LIG sea-level highstand in the coastal environment of sampling
432 sites. Firstly, we considered the present-day coastal marine waters of the Canary Islands.
433 Seawater sampled at 1 m to 5 m depth from Lanzarote and Fuerteventura (Figure 1b) has
434 comparable $\delta^{18}O$ V-SMOW values, 1.09±0.04‰ and 1.08±0.07‰, respectively (Clauzel et
435 al., 2019). Secondly, we calculated the oxygen isotope composition of the LIG global ocean
436 by taking into account the sea-level change relative to present-days. Dutton et al. (2015a)
437 assumed a mean seawater elevation of 7.6 m with respect to the Holocene level that was due
438 to the melting of ice caps with a contribution of +2.0 m from Greenland + 4.6 m from
439 Antarctica, +0.6 m from the glaciers, and +0.4 m from the thermal expansion of the oceans.
440 Goelzer et al. (2016) proposed similar values of +1.4 m for Greenland, +4.4 m for the
441 Antarctica, and +0.4 m for the thermal expansion of the oceans, the contribution of glaciers
442 not being taken into account in this study. The $\delta^{18}O$ of ice in the Greenland Ice Core Project
443 (GRIP) and North Greenland Ice Core Project (NGRIP) ice cores (North Greenland Ice Core
444 Project members, 2004), located on the ice cap plateau, enable us to estimate for the
445 Greenland ice cap an average $\delta^{18}O$ value of about -40.0±2‰. From the data of EPICA Dome
446 C (EDC) and Dome F (Fuji) ice cores (e.g., Landais et al., 2007, and Dome Fuji Ice Core

Project Members, 2017, respectively), located on the ice cap plateau, we evaluate to a first approximation the mean $\delta^{18}O$ of the Antarctic ice sheet at about -57.5±2‰. Consequently, considering a sea-level higher by 7.6 m (Dutton et al., 2015a) during the highstand period of the LIG (±1.5 m), the present-day average ocean depth of 3682±44 m (Charette and Smith, 2010), and neglecting the glacier contribution, a mass balance calculation indicates that the contemporaneous seawater of the molluscs investigated was 0.09±0.02‰ lower than at present. Finally, as we consider that the melting of the ice caps is the main source of $\delta^{18}O$ variation in coastal seawater in the Canary Archipelago between the LIG and now, the $\delta^{18}O$ (V-SMOW) of Lanzarote and Fuerteventura coastal seawaters were likely close to 1.00±0.06‰ during the LIG sea-level highstand. In using Equation (1), a correction of -0.27‰ was applied to convert $\delta^{18}O$ of seawater from the V-SMOW to V-PDB scales according to Bemis et al. (1998) and established by Hut et al. (1987).

4.4. Estimation of the uncertainties

There are different sources of uncertainty associated with the calculation of the SST values. We shall consider first the uncertainties in the two equation variables, $\delta^{18}O_{ar}$ and $\delta^{18}O_{sw}$ (see Equations (1), (2) and (3)). The external reproducibility of $\delta^{18}O_{ar}$ measured from the mollusc shells (±0.10‰) gives an error of ±0.5°C. The error associated with $\delta^{18}O_{sw}$ of coastal seawater in the Canary archipelago during the LIG (≈±0.06‰) is ±0.3°C. Consequently, the uncertainty range in the SST reconstruction is ±0.6°C. This is the uncertainty stated in the results. It is calculated as follows:

$$\square_{total} = \sqrt{(\square_{ar})^2 + (\square_{sw})^2} = \sqrt{(0.5)^2 + (0.3)^2} 0.6 \quad (5)$$

We now consider the uncertainty associated with the linear regression of the empirical data (y = mx+b), which establishes the isotopic fractionation equation for oxygen in the aragonite-water system (Equation (1) and Equation (2)). This uncertainty is not available in the original publications. We used the "lm()" and "pred()" functions of R language (Chambers and Hastie, 1992) and obtained ±0.8°C for the Grossman and Ku (1986) equation (Eq.(1)) and ±0.3°C for the Kim et al. (2007b) equation (Eq.(2)).

5. Results

5.1. Oxygen isotope compositions of the mollusc shells

The bulk sampling method delivers an average signal over the entire life of the specimen. The bulk oxygen isotope data for the two sites of La Santa, Lanzarote (n = 27) and Matas Blancas, Fuerteventura (n = 3) range from -0.14 ‰ to 0.97 ‰ (V-PDB) with a mean value of 0.36±0.27 ‰ (Table S1, in the Supplementary materials).

Incremental sampling yields discrete signals of different periods of the shell growth (younger to older periods). Both the bivalve specimen (*Cardium edule* or *Cerastoderma edule*) from La Santa (n = 1) and the gastropod specimen (*Stramonita haemastoma*) from Matas Blancas (n = 1) show pseudo-cyclic variations of their oxygen isotope compositions recorded during shell growth. The *Cardium edule (Cerastoderma edule)* fossil shell has oxygen isotope ratios ranging from -0.11 ‰ to 2.54 ‰ with a mean value of 1.18±0.72 ‰ while the *Stramonita haemastoma* fossil shell has oxygen isotope ratios ranging from -0.52 ‰ to 0.66 ‰ with a mean value of 0.07±0.36 ‰ (Table S2). A signal drift is observed during the ontogenetic evolution of *Cardium edule (Cerastoderma edule)* with decreasing isotopic compositions from the younger (≈2‰) to the older (≈0.5‰) parts of the shell (Figure 8). The

497 particularly high $\delta^{18}O$ values for the younger part of the record lies outside the range of
498 variation of the other recordings, i.e., the 30 bulk samples and the *Stramonita haemastoma*
499 incremental sample. No such drift is observed during the ontogenetic evolution of *Stramonita*
500 *haemastoma.*
501
502 5.2. Carbon isotope compositions of the mollusc shells
503
504 The bulk carbon isotope data for La Santa and Matas Blancas sites (n = 30) range from
505 1.48 ‰ to 3.40 ‰ (V-PDB) with a mean value of 2.46±0.57 ‰ (Table S1).
506 For the incrementally-sampled specimens, $\delta^{13}C$ of *Cardium edule (Cerastoderma*
507 *edule)* range from 0.51 ‰ to 3.02 ‰ with a mean value of 2.04±0.74 ‰ (n = 1), while $\delta^{13}C$
508 of *Stramonita haemastoma* range from 1.19 ‰ to 3.06 ‰ with a mean value of 1.98±0.50 ‰
509 (n = 1) (Table S2). For the mollusc *Stramonita haemastoma*, the two-tailed probability P
510 calculated at a 95% level of confidence is 0.976 (n = 28; r = 0.0068) thus rejecting the null
511 hypothesis that states there is a correlation between the $\delta^{13}C$ and $\delta^{18}O$ of shell aragonite while
512 in the case of *Cardium edule (Cerastoderma edule)*, the two-tailed probability P calculated at
513 a 95% level of confidence is 0.0014 (n = 16; r = 0.7275) confirming that both variables are
514 significantly correlated (Figure 9).
515
516 5.3. Paleo-temperature reconstructions of coastal seawater
517
518 5.3.1. Mean annual SST during the LIG sea-level highstand
519
520 Marine molluscs living in tropical environments grow all year round and record
521 variations in temperature or salinity at the daily scale (e.g. Frank, 1969). Lifespan for most

522 marine molluscs, and especially bivalves, is lower than 11 years. The data compiled by Moss
523 et al. (2016) reveal that populations of tropical (less than 30° in latitude) bivalves record a
524 mean Maximum reported LifeSPan (MLSP) of 7.9 years, whereas those living under higher
525 latitudes have a mean MLSP of 24.7 years. Therefore, the bulk sampling of mollusc shells
526 delivers an average isotopic record integrated over the entire growth period of the specimen
527 and whose duration is commonly several years. Finally, temperatures calculated from the $\delta^{18}O$
528 of bulk shells are considered to represent the mean annual SST. The data are listed in Table
529 S1, in the Supplementary materials.
530 For La Santa and Matas Blanca sites taken altogether (30 samples), we obtain an
531 average SST of 22.2±1.2°C according to the Grossman and Ku (1986) equation (Eq. (1)) and
532 20.4±1.3°C according to the Kim et al. (2007b) equation (Eq.(2)) (Figure 10). The standard
533 deviation is ≤ ±1.3°C and the SST follow a normal distribution according to the use of
534 normal probability plots with regression coefficients of 0.985. This indicates the sampling of
535 a homogenous assemblage of molluscs, representative of their living environment during the
536 sampling interval, which corresponds to the duration of the LIG sea-level highstand. In
537 summary, values of 22.2±1.2°C (Eq. (1)) and 20.4±1.3°C (Eq. (2)) represent an average SST
538 coming from 30 molluscs whose deposit extends over several thousand years (≈125 to 119-
539 116 ky BP), each sample providing a mean annual SST value over a few years of life.
540
541 5.3.2. Seasonal SST during the LIG sea-level highstand
542
543 As the incremental sampling gives access to different periods recorded during the
544 growth of the mollusc shell, it could potentially allow seasonal temperature variations to be
545 reconstructed. Sclerochronological studies performed on modern bivalve molluscs show that
546 they form patterns of periodic annual banding in their shell (Butler and Schöne, 2016).

Moreover, image processing by Scanning Electron Microscopy (SEM) on the outer surface of modern bivalve *Cerastoderma edule* shells from high latitudes (North Sea, 55°N) show that winter and summer growth lines are consistent with $\delta^{18}O$ variations from shell incremental measurements, higher $\delta^{18}O$ values corresponding to cold water conditions (≈10°C) and lower $\delta^{18}O$ values to warm water conditions (≈22°C) (Milano et al., 2015). Data from *Stramonita haemastoma* (Matas Blanca) (Figure 11) and *Cardium edule (Cerastoderma edule)* (La Santa) (Figure 12) (2 samples) show a pseudo-cyclical SST record, particularly obvious for *Stramonita haemastoma*. The variations, of sinusoidal type, are distorted in the ontogenic profiles since the exoskeleton growth mode of many molluscs follows a logarithmic law (Cornu et al., 1993; Roman-Roman et al., 2010). Mean temperatures reconstituted from the $\delta^{18}O$ of shell increments from the *Stramonita haemastoma* specimen collected at Matas Blanca, Fuerteventura, and the *Cardium edule (Cerastoderma edule)* specimen collected at La Santa, Lanzarote, are between 23.5±1.6°C and 21.8±1.8°C and between 18.7±3.1°C and 16.6±3.3°C, respectively, according to Equation (1) and Equation (2). The first set of temperatures is close to those obtained for the 30 bulk samples, while the second set is much lower and displays a wide distribution (standard deviation of more than 3°C) due to the $\delta^{18}O$ signal drift (§5.1).

For the gastropod *Stramonita haemastoma*, about 4 seasonal SST cycles are observed over a total length to apex of 16 cm (Figure 11) with variations in SST comprised between ≈3.5°C and ≈5.5°C. For the bivalve *Cardium edule (Cerastoderma edule)*, we observe SST fluctuations that mimic a seasonal-like signal recorded over two or more cycles, over a total length to umbo of 4.5 cm (Figure 12). Due to a signal drift (§5.1), we focus here on the oldest biological age of the mollusc shell. The average SST comprised between 21.1±1.6°C (Eq. (1)) and 19.2±1.8°C (Eq. (2)) is consistent with the average temperature reconstructed from the 30 bulk samples. The seasonal SST fluctuation is approximately 6.0°C. We note that this

SST amplitude is also observed for the youngest part of the mollusc shell. The low SST values recorded by the youngest part of the *Cardium edule (Cerastoderma edule)* shell, caused by the $\delta^{18}O$ signal drift, could result from an inter-annual fluctuation of the SST, with particularly cooler marine waters during the first period of life of the mollusc sample, a period that may last for 1 or 2 years. Finally, seasonal SST values during the LIG sea-level highstand, established from two samples with a lifespan of a few years, range from ≈3.5°C to ≈6.0°C.

6. Discussion

6.1. Interpretation of the fossil faunal record

The ecology of the species present in the LIG marine deposits indicates that they lived in different types of environments (§3.1) that can be designated as (a) warm water environments, (b) warm and cooler water environments and (c) cooler water environments (Figure 5).

The co-occurrence of these different faunal groups in the LIG fossil record can be understood as follows. The marine deposits accumulated throughout the second part of the LIG, a period when the warm climate became progressively cooler, similar to that observed during the second part of the Holocene (Marcott et al., 2013). The whole LIG marine deposit therefore consists of both "warm fauna", corresponding to the warm phase of the second part of the LIG, and "cooler fauna", corresponding to the end of the LIG, before the sea-level fell and the sediment accumulation stopped. Firstly, during the LIG warming, the "warm species" or extralimital southern species (Muhs et al., 2014) migrated from low latitudes up to latitudes as far as the Mediterranean sea (Muhs et al., 2014). Secondly, when the SST decreased,

extralimital southern species disappeared in the Canary Islands. This scenario of faunal shifts during the LIG in the Canary Islands was also documented by Muhs et al. (2014), but whereas they deal with the whole of the LIG period, here, we consider only the sequence of sediment deposits, i.e., the second part of the LIG. It follows that in principle the first arrival of the "warm species" is not recorded in our marine deposits.

These faunal changes are illustrated by the presence of *Persististrombus latus (Strombus bubonius)*, known as a Guinean-Senegalese taxon, in the samples we collected in the Matas Blancas deposit, i.e., north of its present geographical distribution. This observation indicates that during the LIG the SST was higher than in the present interglacial, as already noted by Muhs et al. (2014). This finding is consistent with the particularly high and reproducible LIG SST values recorded for the 3 specimens of *Persististrombus latus* , namely 23.4±0.5°C (Eq.(1)) and 21.7±0.6°C (Eq.(2)) (see Table 2). These values are clearly higher by about +1.2°C than the mean temperature found for the total bulk sampling (30 samples, §5.3.1), which includes the cooling period at the end of the LIG.

6.2. Interpretation of the mean annual paleo-SST reconstructions

6.2.1. LIG SST anomaly with respect to pre-industrial times

As in the first step, where the mean annual SST was estimated from mollusc shell $\delta^{18}O$ values in the eastern Canary Islands during the LIG, in a second step we estimated the change in SST with respect to pre-industrial times, i.e., the middle of the nineteenth century.

We recall the SST value of 20.4°C in the eastern islands of Canary archipelago for the period from 2007 to 2017 (§2.2).

The recent evolution of air temperature has been evaluated by Martín et al. (2012) from meteorological measurements on Tenerife Island, Canary archipelago. A warming trend of

623 0.09±0.04°C.decade^{-1} between 1944 and 2010 was observed, which increased to
624 0.17±0.04°C.decade^{-1} in the period 1970-2010. At Gran Canaria, Canary archipelago, Luque
625 et al. (2014) observed similar trends over the same periods, respectively. Such acceleration in
626 the temperature rise is consistent with the SST trends from Advanced Very High Resolution
627 Radiometer (AVHRR) and *in situ* data in the eastern Canaries published by Gómez-Letona et
628 al. (2017) who estimated this trend to be about 0.22°C.decade^{-1} during the period 1993–2014.
629 From the estimated SST warming of about 0.2±0.04°C.decade^{-1} since the seventies
630 (Gómez-Letona et al., 2017; Martín et al., 2012; Luque et al., 2014), and the increase in SST
631 of about 0.2±0.05°C between the beginning of the twentieth century to the nineteen seventies
632 based on the GMST trend (IPCC, 2013), we assume that the SST increased by about
633 1.0±0.1°C in the eastern Canaries between the pre-industrial times and the 2010s. This
634 estimate is based on the fact that that global temperature increase observed from the
635 beginning of the pre-industrial until the beginning of the 20th century (IPCC, 2013) is
636 negligible. We therefore assume a pre-industrial SST of the order of 19.4±0.1°C. This result
637 is consistent with the calculated SST value of 19.8°C in 1986 (Borges et al., 2004), which
638 implies a pre-industrial SST of about 19.3°C.
639 Consequently, with respect to pre-industrial times, our results show that the mean SST
640 anomaly that prevailed during the LIG sea-level highstand is comprised between at least
641 +1.0±1.4°C (Equation (2)) and +2.8±1.3°C (Equation (1)) at the two coastal sites of La Santa
642 and Matas Blancas.
643

644 6.2.2. Global and regional LIG temperature distribution
645

646 A full understanding of the context in which the local SST warming took place in the
647 eastern Canary Islands calls for a broad view of the temperature change both on a regional

scale and on a global scale. Owing to coupling between the regional and local scale pattern and the global climate, it is possible to estimate the consistency of our results with the temperature pattern at the LIG. Two strong qualitative pieces of evidence show that the LIG was globally warmer than the Holocene : the amply documented Antarctic polar warming, and the sea-level rise and high-stand above that of the present (+6 to +9 m) (e.g., Table 2, Figure 6). How much warmer the LIG was on Earth at the regional and global scale remains an intensely discussed topic within the paleoclimate community. Nevertheless, some major aspects of this warming can be summarized as follows.

The Past Interglacials Working Group of PAGES (2016) recently published an overview of the climate patterns of the LIG. The different interglacial periods over the last 800 ka were described. The characteristics of the successive interglacials depend on seasonal and latitudinal insolation, which are determined by astronomical parameters (Milankovitch, 1941; Berger, 1988). The time dependence of these parameters explains the markedly warm climate of some interglacial periods, in particular the LIG (e.g., Mélières and Maréchal, 2015). The LIG appears to be the warmest of the last eleven interglacial stages: compared to the Holocene, it was warmer by between 0°C and +4°C depending on the latitude (Past Interglacials Working Group of PAGES, 2016). At the global scale, the LIG global mean surface temperature (GMST) can first be inferred independently from the $\delta^{18}O$ and δD temporal series measurements of ice cores located in the plateau of Antarctica. These ice core records allow us to reconstruct changes in air temperatures above the ice cap. We focus here on the Dome C ice core, which shows an air temperature record consistent with those of three other coring sites at Vostok, Dronning Maud Land and Dome F (see for example Capron et al., 2014). During the LIG, they indicate that, with respect to the mean Holocene temperature, the Antarctic air surface temperature record divides into two periods, in which a peak anomaly of about +4°C around ≈130 ka BP is followed by a plateau type signal of about

673 +2°C between ≈126 ka and ≈119 ka BP (Figure 6c). These local temperatures reflect the
674 regional temperature because the Antarctic plateau is characterized by spatially-equalized
675 climatic conditions. In different studies a linear relationship of GMST change for every 1°C
676 change in Antarctic temperatures across glacial-interglacial cycles is inferred : between 0.5°C
677 (Masson-Delmotte et al., 2010; Chylek and Lohmann, 2008; Hansen et al., 2008) and 0.6°C
678 (Snyder et al., 2016). We can therefore estimate a maximum GMST anomaly of at least
679 ≈+2°C around ≈130 ka BP, followed by a plateau type temperature signal of at least ≈+1°C
680 between ≈126 ka and ≈119 ka BP. Our samples are therefore contemporaneous with a period
681 defined by a GMST warmer than present by about +1°C relative to the mean Holocene
682 temperature. These GMST anomalies are consistent with the estimates of Snyder et al. (2016)
683 and Hansen et al. (2013), which are based on a broader time scale. Snyder et al. (2016) used a
684 multi-proxy database compilation to reconstruct the GMST over the last 2 Ma: they found
685 that during the LIG the GMST was +2°C warmer than in the late Holocene (0-5 ka BP).
686 Finally, Hansen et al. (2013) reconstructed the GMST over the last 65 Ma and calculated that
687 the LIG was +1.4°C higher than during the Holocene. Regarding exclusively the global sea
688 surface temperature, a warming of +0.5°C±0.3°C at 125 ka with respect to the pre-industrial
689 times has been reported by Hoffman et al. (2017).

690 Focusing now on regional changes, during the LIG the Arctic region was consistently
691 warmer than today. The CAPE-Last Interglacial Project Members (2006) offered quantitative
692 estimates of circum-Arctic LIG summer air and sea surface temperatures (SST), reconstructed
693 from proxies inferred from terrestrial and marine records. These reconstructions indicate that
694 Arctic summer air temperatures were on average about +4 to +5°C higher than at present for
695 most of the Arctic, well above the planetary LIG average. A synthesis of temperature data
696 obtained at different climatic time slices at 125 ka BP and 120 ka BP indicates that the highest
697 temperature was about +4°C to +5°C warmer than present in central Greenland (Capron et al.,

2015, 2014). Regarding continental data obtained at mid latitudes in the northern hemisphere, Kaspar et al. (2005) compared the anomalies between reconstructed January and July temperatures for a 125 ka time slice and present-day observed temperatures in Europe. Their reconstructions, based on pollen and plant macrofossils, indicate warming by a few degrees. Brewer et al. (2008) report climate reconstructions from across the European continent. Their results show a traditional three-part LIG, with an early optimum, followed by a slight cooling stage and finally a sharp drop in temperature. The climate anomalies were mapped for four periods (127 ka, 123 ka, 117 ka, 109 ka BP). Maximum warming took place at 127 ka BP, a period during which the climate anomalies ranged from +4°C in northern Europe to +1°C in the south of France.

Concerning the sea surface temperature, Capron et al. (2017a) published a critical evaluation of data compilation at high latitudes. These authors emphasise that all high-latitude regions experienced warmer conditions at the 125 ka time slice relative to the present-day, with temperature anomalies reaching +1.6±0.5°C and +0.8±0.5°C in the North Atlantic and in the Southern Ocean, respectively. In the last decades, global syntheses have been performed, first by Turney and Jones (2010) and by McKay et al. (2011). McKay et al. (2011) suggest a peak in the LIG global annual SST warming of +0.7±0.6°C with respect to Late Holocene (5 to 0 ka BP). Both compilations indicate a general warming at high and middle latitudes but, for the tropics, a less consistent pattern emerges in which SST cooling is identified in the tropical Atlantic Ocean. However, Capron et al. (2017b) suggest that these two LIG data syntheses may have major methodological limitations related to the chronology. Recently, Hoffman et al. (2017) published a new LIG SST compilation of global extent with a consistent temporal framework. The temperature anomalies with respect to 1870-1889 are estimated for three different time slices during the LIG (129, 125 and 120 ka BP). Three world maps of proxy-based mean annual SST anomalies at the LIG, based on 83 marine

723 sediment core sites, were established using temperature estimates from Mg/Ca in planktonic
724 foraminifera, $U^{K'}_{37}$ from alkenones, and microfossil reconstructions. For each time window,
725 significant cooling by a few degrees at the LIG took place in the tropical north Atlantic Ocean
726 and along the west African coast. At the global scale, as already noted, SSTs reached
727 +0.5°C±0.3°C at 125 ka.

728 All the above estimates concur to show that the GMST at LIG was on average
729 higher than during the Holocene. This warming was not uniform, but increased towards the
730 poles. Some oceanic regions, however, did not follow this rule, as suggested by SST
731 reconstitutions performed in the North Tropical Atlantic Ocean by Hoffman et al. (2017). In
732 particular, the waters of the tropical Atlantic gyre, whose descending branch, the Canary
733 Current, bathes the West African coast, appeared to be cooler.

734 Turning now to the regional scale, in the northeast tropical Atlantic area where the
735 Canary Islands are located, a few studies aim to reconstruct the SST during the LIG (Figure
736 3b, Table 3). Sicre et al. (2000) analysed terrigenous and marine biomarkers from a core
737 (SU94-20bK) that recorded the last 150 ka in the northeast Atlantic off Northwest Africa at
738 25°00.60'N, 16°23.40'W. Their results from $U^{K'}_{37}$ analyses revealed an annual SST of 23.3°C
739 during the LIG (from ≈128 to ≈120 ka BP) and 21.8°C during the beginning of the
740 Holocene, thereby indicating an anomaly of +1.5±0.3°C during LIG with respect to the core
741 top (dated at ≈9 ka BP). Matsuzaki et al. (2011) studied a core (MD03-2705) retrieved off
742 the Cape Verde Islands at 18°05.81'N, 21°09.19'W, spanning the last 220 ka. The annual SST
743 anomaly estimated from planktonic foraminifera assemblages between LIG (from ≈122 to
744 ≈118 ka BP) and the core top (dated at ≈10-8 ka BP) is +0.5±0.6°C. Castañeda et al. (2009)
745 analysed a sediment core (GeoB9528-3) retrieved from the Guinea Plateau Margin at
746 09°09.96'N, 17°39.81'W, spanning the last 192 ka. The $U^{K'}_{37}$–based annual SST gives a LIG
747 anomaly value of +1.0±0.5°C (from ≈125 to ≈120 ka) with respect to the core top (dated at

748 ≈9 ka). The SST anomalies from these studies (Sicre et al. (2000), Matsuzaki et al. (2011),
749 Castañeda et al. (2009)) with respect to the core top values are displayed in Figure 13a. These
750 values can be expressed relative to pre-industrial times by taking into account the results of
751 the two following investigations. Fischer et al. (2018) indicate a cooling of the global surface
752 air temperature by ≈0.7±0.3°C between ≈9 ka BP and the period 1850-1900. The same
753 order of magnitude is obtained from Arbuszewski et al. (2013). In order to obtain the SST
754 anomalies with respect to the pre-industrial times, the value of 0.7°C must therefore be added
755 to the core top values (Figure 13b). Turning now to the evidence from coastal molluscs, Muhs
756 et al. (2014) noted a dramatic warming of marine waters around the Canary Islands during the
757 LIG, on the basis of on the presence of 16 exclusively extralimital southern species found in
758 their LIG deposits. At present, these species live between the Cape Verde Islands and south
759 Angola and are members of the tropical Senegalese-Guinean faunal province. During the LIG
760 one of the most celebrated Senegalese taxa, *Persististrombus latus (Strombus bubonius)*
761 (Figure 4), was distributed between Cape Verde Islands and the Mediterranean region. The
762 geographic extent of these extralimital southern species during the LIG indicates that these
763 numerous mollusc species migrated northwards during the LIG, a situation that requires
764 warmer waters than at present. Montesinos et al. (2014) estimated the SST anomaly around
765 the Canary Islands by comparing the present geographical distribution of an extralimital
766 southern warm-water species, *Harpa doris* Röding, 1798 (*Harpa rosea*), with that prevailing
767 during the LIG. This estimate is based on the presence of *Harpa doris* in marine deposits
768 from the Canary Islands (Gran Canaria, Lanzarote and Fuerteventura) during the LIG. This
769 mollusc disappeared from the Canary Islands after the LIG and has not reappeared since.
770 Today, *Harpa doris* lives far to the south in the Gulf of Guinea, from Angola to Senegal.
771 Comparison between the annual SST of the present habitat of *Harpa doris* and the annual
772 SST of the Canary Island coasts enabled Montesinos et al. (2014) to evaluate a surface

773 temperature anomaly at LIG of at least +3.3°C higher than today. To relate this value to the
774 pre-industrial period, we applied the correction method described in § 6.2.1. Since
775 Montesinos et al. (2014) took the 2000s as the reference date for the present period, we
776 assume the increase in SST in the Canary Islands from the pre-industrial to the 2000s to be
777 about 0.8°C. The annual SST anomaly is therefore at least +4.1°C higher than in pre-
778 industrial times. This value spans the LIG marine deposit period that we estimated to be
779 between ≈125 and 119-116 ka BP (§ 3.2) (Figure 13b). Finally, the compilation work of
780 Hoffman et al. (2017) includes three cores located in the tropical Northeast Atlantic region:
781 GIK15637 (27°00.00'W, 18°58.80'W), M12392-1 (25°09.60'W, 16°51.00'W), and V22-196
782 (13°49.80'N, 18°58.20'W), where foraminiferal assemblage-based annual SST anomalies
783 with respect to the pre-industrial times (1870-1889) for three different time slices during the
784 LIG (129, 125 and 120 ka BP) are deduced from the three maps shown. The values range
785 from -4.8±0.5°C to +0.3±0.5°C (estimated from the color code of the maps).
786
787 6.2.3. LIG SST data comparisons
788
789 Our results for the coastal surface waters during the second part of the LIG recorded in
790 Lanzarote and Fuerteventura indicate a positive temperature anomaly comprised between
791 +1.0±1.4°C and +2.8±1.3°C with respect to pre-industrial times. This positive anomaly,
792 obtained from geochemical analyses of mollusc shells in LIG marine deposits, is congruent
793 with data obtained from the northeast tropical Atlantic by two other methods, namely analyses
794 of microfossils and alkenones in deep-sea cores (Sicre et al., 2000 ; Matsuzaki et al., 2011 ;
795 Castañeda et al., 2009) and analyses of mollusc assemblages in LIG marine deposits (Muhs et
796 al., 2014 ; Montesinos et al., 2014) (Figure 13b). The relatively strong SST anomaly in the
797 Canary Islands reported by Montesinos et al. (2014) is consistent with the qualitative study of

798 Muhs et al. (2014), which covers a wider geographical area stretching as far as the
799 Mediterranean and includes a larger number of taxa. All of these studies clearly indicate a
800 warming in the second part of the LIG with respect to pre-industrial times.

801 However, such positive temperature anomalies appear to conflict with the compilation
802 of Hoffman et al. (2017) for the North Atlantic tropical SST, where two of the three cores
803 reported indicate colder surface waters during the LIG with respect to pre-industrial times.
804 The amplitude of these negative temperature anomalies differs according to the LIG time
805 slices studied. We exclude the beginning of the LIG (129 ka BP), which could be affected by
806 glacial-interglacial transition mechanisms (e.g., Capron et al., 2014). At 125 ka BP, only one
807 core (M12392) exhibits significant cooling of -3.0±0.5°C. At 120 ka BP, two cores (M12392,
808 V22-196) indicate negative SST anomalies of -3.0±0.5°C and -1.5±0.5°C, respectively. The
809 SST anomalies from these cores are less convincing when the core-top SST value
810 reconstructed for the Holocene is taken into account (Hoffman et al., 2017; Hessler et al.,
811 2014) : the absence of original SST data in the core-top (CLIMAP, 1984) prevents accurate
812 comparison of the SST with respect to the Holocene. For this reason, the few data points that
813 display negative LIG temperature anomalies in the compilation by Hoffman et al. (2017) may
814 not be reliable. Furthermore, they are inconsistent with the warmer surface waters
815 documented by the other investigations in the region, as well as with the results of our present
816 study.

817 Our evidence therefore points to a warming of the SST off Northwest Africa from ≈125
818 ka to ≈119-116 ka BP with respect to pre-industrial times. This warming, which only
819 concerns the second part of the LIG, is in principle weaker than that of the first part of the
820 interglacial, where the insolation was maximum. It therefore indicates a lower value of the
821 temperature anomaly for the LIG (129 ka to 116 ka). One possible cause of this warming
822 could have been weakening of the North African upwelling, which would increase the SST.

The warming could also be due to the high insolation during the LIG, thereby warming the Canary Current from the North Atlantic gyre.

6.2.4. Upwelling impact and insolation effect

To understand the potential impact of climate change on the coastal upwelling activity, further information is needed about how it changed during the different climatic alternations between recorded warming and cooling events in the past (interglacial and glacial periods, respectively). For the Holocene period, the summer insolation in the northern hemisphere slowly decreased, resulting in a slow diminishing of the GMST and a reduction in summer monsoon activity in the northern tropical regions of Africa (deMenocal et al., 2000; Shanahan et al., 2015; Collins et al., 2017), Asia and North America (Wang et al., 2009). The global Earth climate, which was initially warm and humid, became cooler and drier, with a transition at around 5 ka BP. Re-interpretation of two SST proxies at ODP Hole 658C, off Cape Blanc (20°45'N, 18°35'W, south of the Canary Islands, see Figure 1) combined with new data, provided a better understanding of the history of upwelling of North Africa (Adkins et al., 2006). These authors concluded that weaker upwelling activity coupled with stronger African monsoon activity occurred during the African Humid Period in the first part of the Holocene. A similar observation was made by Abrantes (1991) who documented a warming period in the region of the Canary Islands that spanned several millennia in the first part of the Holocene, accompanied by a reduction in the intensity of the northwest African upwelling. During the LIG, such a weakening of the upwelling is also suggested by Muhs et al. (2014) from the faunal record in the Canary Islands. The LIG may have been characterized by early insolation-forced warming along with northward migration of the intertropical convergence zone (ITCZ), and accompanied by weakened trade winds and diminished upwelling. This

allowed the arrival of extralimital southern taxa from the tropical Senegalese faunal province. During the latter part of LIG, decreased insolation may have resulted in southward migration of the ITCZ, strengthened trade winds, and re-establishment of the upwelling. Such conditions may have brought about the local extinction of the Senegalese fauna. The change of the upwelling strength can also be documented in the framework of larger climate changes, such as glacial and interglacial oscillations. Those oscillations extend over millennia, the cyclic climate alternation driven by variations in the summer insolation at middle to high latitudes in the northern hemisphere. Although the boundary conditions of the climate in the LGM and the LIG were different, they were both the result of insolation changes, and these modulate atmospheric circulation and hence the upwelling strength. The global warming that took place from the LGM to the Holocene was of the order of +5°C (Masson-Delmotte et al., 2013; Snyder, 2016). Henderiks et al. (2002) estimated the changes in the Canary seasonal coastal upwelling from LGM to the Holocene : they documented stronger trade winds and enhanced productivity during the LGM, in good agreement with previous studies of the northwest African upwelling and trade wind-system (e.g., Sarnthein et al., 1982, 1988; Abrantes, 1991; Rognon and Coude-Gaussen, 1996). Similar observations, but spanning a larger time scale, were made by Freudenthal et al. (2002), who reconstructed changes in trade wind intensities over the last 250 ka at 4 sites close to the Canary Islands. Furthermore, from a sediment core in the Canary Basin, Nave et al. (2003) indicated that the glacial stages MIS4 and MIS2 were more productive than the interglacial intervals (LIG and Holocene). Moreno et al. (2002) analysed the primary productivity record from sediment cores over the last 250 kyr in the North Canary Basin (30°N). Their work demonstrates that productivity is lower during interglacials than during glacial periods. These observations corroborate the fact that in glacial times the northwest Africa coastal upwelling activity increased. All of the above observations indicate a weakening of upwelling activity during periods of global warming.

873 We therefore conclude that the North African upwelling was weaker during the LIG than
874 during the Holocene. This finding implies warmer coastal seawater during the LIG relative to
875 the Holocene.

876 The maximum increase in SST attributable to a weakened upwelling can be estimated
877 from the present-day isotherms of the eastern Atlantic tropical gyre. Upwelling only decreases
878 the SST along the coast (Figure 3b). According to recent data, in the eastern Canary Islands
879 this cooling ranges from 0.75°C to 1°C (Gómez-Letona et al., 2017 ; Sousa et al., 2017 ;
880 Santos et al., 2012 ; Arístegui et al., 2009 ; Muhs et al., 2014, after Conkright et al., 2002). It
881 follows therefore that a weakening of the upwelling will lead to a warming by between
882 0.75°C and 1°C at the very most, since the cold deep waters never completely stop rising.
883 However, the increase in SST with respect to pre-industrial times, indicated by proxies from
884 the upwelling zone off northwest Africa (excluding the values of Hoffman et al., 2017) is
885 significantly greater. It lies in the range +1°C to +4°C (Figure 13b). As such a temperature
886 rise is too large to be attributed to a weaker upwelling alone, an alternative and additional
887 mechanism, namely the insolation at the LIG, must therefore be examined.

888 *Summer insolation* in the northern hemisphere, the main driving force of the glacial-
889 interglacial oscillations, was more pronounced during the LIG than in the Holocene, leading
890 to an interglacial that was on average warmer (CAPE-Last Interglacial Project Members,
891 2006; Masson-Delmotte et al., 2013; Capron et al., 2014). Between 30°N and 90°N the
892 insolation anomaly 125 ka ago exhibited a maximum in July between ≈+50 W/m^2 and ≈+70
893 W/m^2 with respect to pre-industrial times (Pedersen et al., 2016). These results are in
894 agreement with those of Capron et al. (2017b). Not only the *summer insolation* but also the
895 *annual insolation* anomaly was positive (between 0 and +2.5 W/m^2) (Pedersen et al., 2016).
896 By contrast, the *annual insolation* anomaly observed in the tropical latitude belt between
897 30°N and 30°S displayed a slight decrease comprised between 0 and -0.2 W/m^2 (Pedersen et

al., 2016). It is to this *annual insolation* decrease in the tropical latitudes that Hoffmann et al. (2017) attributed their estimated cooling of the SST in the tropical Atlantic. According to the latter authors, the simulations of Pedersen et al. (2016) at 125 ka "successfully simulate the weak cooling found in our tropical SST stack in response to reduced mean *annual insolation* at those latitudes". However the simulations performed by Pedersen et al. (2016) revealed *annual cooling* of the air temperature only in the continental tropical zones of North Africa (5°N-20°N) and Asia (India). The tropical north Atlantic not only does not exhibit cooling but rather a *warming* of between +0.5°C and +3°C, and in particular a warming of between +1 and +3°C in its north-eastern part from 22°N to 30°N with respect to pre-industrial times. Pedersen et al. (2016) attribute the continental cooling to the impact of *summer warming* in the Northern hemisphere, which amplified the North African and Indian monsoons. Owing to this amplification, evaporation and spread of the cloud cover became more pronounced, consequently cooling the continental surface. The continental cooling was thus mainly caused by the increase in seasonal *summer insolation*, rather than being due to a reduction of the *annual insolation* in the tropics. Accordingly, in spite of the reduced *annual insolation* that took place in the tropics during the LIG, the simulation of Pedersen et al. (2016) did not reproduce the cooling indicated by Hoffman et al. (2017) in the north-east tropical Atlantic. On the contrary, it reveals warming of the surface water in the northern tropical Atlantic, in agreement with our own measurements as well as with the majority of compilations conducted in this zone. These results lend support to the impact of summer insolation in the Northern hemisphere on the SST of the Canary current water masses during the LIG. The warming by about +1°C to +4°C (Figure 13b) of the SST in the tropical northeast Atlantic, reported by all the data sets, apart from those reconstituted by Hoffman et al. (2017), thus stemmed principally from the excess *summer insolation* during the LIG and, to a lesser degree, from a weakening of the upwelling. Therefore this indicates a warming of the

descending branch of the North Atlantic Gyre (Canary current), mainly engendered by the larger summer insolation. As the descending branch is part of the gyre, this implies that the warming extended over the whole of the gyre.

6.3 Seasonal variations in paleo-SST and paleo-Dissolved Inorganic Carbon (DIC) $\delta^{13}C$

6.3.1. Seasonal SST during the LIG sea-level highstand

According to the SST inferred from incremental sampling of two specimens with a lifespan of a few years, which are the gastropod *Stramonita haemastoma* sampled from Matas Blancas, Fuerteventura, and the bivalve *Cardium edule (Cerastoderma edule)* sampled from La Santa, Lanzarote, the pseudo-cyclic SST pattern observed along the growth direction of the shells can be attributed to the seasonality of the SST. Those two mollusc shells recorded seasonal SST variations ranging from ≈3.5°C to ≈6.0°C, with a mean value of about 4.8±1.2°C, during the LIG sea-level highstand (≈125 to ≈119-116 ka BP) in the eastern Canary archipelago. Other LIG seasonal SST values for the northeast Atlantic region may be deduced from the difference between the winter mean SST (JFM) and the summer mean SST (JAS) reconstructed from foraminifera assemblages, by a method that is complementary to our approach based on stable oxygen isotope compositions of carbonates. Indeed, Matsuzaki et al. (2011) estimated seasonal SST variations to be about 5.0±1.2°C during the second part of the LIG, from ≈122 to ≈118 ka BP, from the core MD03-2705 (Figure 3b) located in the northeast of Cape Verde Islands (18°05.81'N, 21°09.19'W). From the cores M12392-1 south of the Canary archipelago (25°09.60'W, 16°51.00'W) and V22-196 between the Cape Verde Islands and Senegal (13°49.80'N, 18°58.20'W) (Figure 3b) (CLIMAP Project Members, 1984), seasonal SST variations were estimated to be ≈5.0±2.4°C and ≈5.5±2.6°C during the

LIG, respectively. The core top of those two cores, which is not available, is not necessary for these calculations. All these LIG seasonal SST estimates in the northeast Atlantic region match our values.

Meco et al. (2018) reported a seasonal SST amplitude along the eastern coast of Fuerteventura ranging from 3.5°C to 6.7°C between 2007 and 2016. The seasonal temperature variations from ≈3.5°C to ≈6.0°C recorded by the two mollusc shells, *Stramonita haemastoma* and *Cardium edule (Cerastoderma edule)*, during the LIG sea-level highstand in the eastern Canary Islands are therefore comparable to those of modern times. Finally, our data obtained from mollusc samples and those coming from the cores MD03-2705, M12392-1 and V22-196 indicate that the SST seasonality of the northeast Atlantic waters was of the same order during the LIG as that of present-days.

6.3.2. Mean annual and seasonal DIC $\delta^{13}C$ during the LIG sea-level highstand

Coastal upwelling areas are important dynamic parts of the ocean carbon cycle. The bulk carbon isotope data for La Santa and Matas Blancas sites provide a mean $\delta^{13}C$ value of 2.46 ± 0.57 ‰ (Table S1, in the Supplementary materials). This value represents an average of 30 mollusc shells from a LIG sedimentary deposit that extends over several thousand years, each sample being characterized by a multiannual $\delta^{13}C$ value. Several authors (e.g. Mackensen et al., 1993; Rohling and Cooke, 1999; Maslin and Swann, 2005) have shown that the $\delta^{13}C$ value of biologically precipitated carbonate in seawater is very close to that of Dissolved Inorganic Carbon (DIC). Therefore the $\delta^{13}C$ values recorded in the aragonite mollusc shells should represent that of seawater DIC. As emphasized by Maslin and Swan (2005), the $\delta^{13}C$ values of planktonic carbonate foraminifera increase with higher biological productivity. This is due to isotope fractionation during the photosynthesis process where the

973 lighter $^{12}CO_2$ is preferentially selected by the organic matter, thereby leaving the surface water
974 DIC enriched in ^{13}C. Thus, the positive mean annual $\delta^{13}C$ values of carbonate shells from the
975 eastern Canary archipelago reflect a high marine productivity of surface waters during the
976 sea-level highstand, i.e., from ≈125 ky to 119-116 ky BP (Maslin and Swan, 2005).

977 The mollusc shells selected for isotopic ontogenetic profiles provide complementary
978 information at the seasonal scale of the $\delta^{13}C$ values of DIC. We consider that the $\delta^{13}C$
979 fluctuations recorded in the aragonite mollusc shell represent the $\delta^{13}C$ fluctuations of seawater
980 DIC. $\delta^{13}C$ values of the incrementally sampled shell of *Cardium edule (Cerastoderma edule)*
981 sampled from La Santa sedimentary sequence show a pseudo-cyclic signal recorded over a
982 few years, with $\delta^{13}C$ values ranging from 0.51 ‰ to 3.02 ‰ (Table S2, in the Supplementary
983 materials). These values, obtained from one sample, range around a mean value
984 (2.04 ± 0.74 ‰) similar to the mean annual $\delta^{13}C$ averaged over several thousands of years
985 during the LIG (2.46 ± 0.57 ‰), which indicates highly productive marine waters. The $\delta^{13}C$
986 values of the incremental samples from the *Cardium edule (Cerastoderma edule)* shell are
987 correlated with those of $\delta^{18}O$, the regression line having a positive slope of 0.73 and a
988 regression coefficient R^2 of 0.51 (Figure 9). At the seasonal scale, these observations mean
989 that the lowest shell $\delta^{13}C$ values correspond to the higher SST values during LIG (Figure S2,
990 in the Supplementary materials). In upwelling areas, the superficial upwelled seawater is
991 characterized by ^{13}C-depleted DIC generated by oxidation of organic matter. This is due to the
992 fact that after the death of phytoplankton, the ^{12}C-enriched organic matter sinks into the deep
993 ocean and is degraded and remineralized. As a result, upwelled deep waters are characterised
994 by ^{13}C-depleted DIC (Peeters and al., 2002). The low values of shell $\delta^{13}C$ therefore indicate an
995 enhanced seasonal upwelling activity. Owing to the recorded correlation between the shell
996 $\delta^{13}C$ values and the SST, the LIG enhanced upwelling activity corresponded to high SST
997 periods, i.e., to summer seasons (Meco et al., 2018). A more active upwelling in summer

998 during the LIG sea-level highstand is consistent with the present enhanced upwelling during
999 summer (Pardo et al., 2011; Navarro-Pérez and Barton, 2001; Mittelstaedt, 1991) (see §2.2).
1000 In one of the most active upwelling areas, the Peruvian upwelling, Sadler et al. (2012) noted
1001 the same relationship between $\delta^{13}C$ DIC recorded by fossil shell $\delta^{13}C$ values and the upwelled
1002 water season, i.e., low shell $\delta^{13}C$ values corresponding to maximum upwelling intensity.
1003 However, unlike the upwelling off western Africa, that off Peru is strengthened in winter, and
1004 accordingly, lower values of shell $\delta^{13}C$ correspond to lower SSTs. We note that as the Canary
1005 Current SSTs are highest during summer (Meco et al., 2018), the main factor controlling the
1006 seasonal variation of SST is the insolation. The thermal impact of upwelling, which decreases
1007 the SST particularly when it is active in summer, however, is only of second order.
1008 The seasonal influence of the Canarian upwelling seems to be only recorded in La
1009 Santa, Lanzarote, and not in Matas Blancas, Fuerteventura, a difference that may be explained
1010 by the geographical location of these two sites. Lanzarote and Fuerteventura are both situated
1011 at the eastern end of the archipelago where the global influence of the upwelling is the
1012 strongest. However, La Santa lies on the western side of the island of Lanzarote while Matas
1013 Blancas is located east of the island of Fuerteventura. Local upwelling always takes place on
1014 the western sides of lands due to the westerly direction of the Trade Winds. The reconstitution
1015 of the pigment content of the surface seawater from satellite recordings (Nave et al., 2001,
1016 2003; Borges et al. 2004), which is a signature of the primary oceanic productivity, indeed
1017 exhibits a local annual coastal upwelling on the western coasts of Lanzarote and
1018 Fuerteventura, and not along the eastern coasts.
1019 Our results suggest seasonal variations in the oceanic surface water parameters of
1020 the Canary archipelago during the LIG related to the SST and to the North African coastal
1021 upwelling activity. These seasonal fluctuations resemble those of the present time.
1022

7. Conclusion

The stable isotope study of aragonitic mollusc shells sampled from the sites of La Santa, Lanzarote, and Matas Blancas, Fuerteventura, in the eastern part of the Canary archipelago reveals several important findings about the climate during the Last Interglacial, the LIG :

(i) The sample collection investigated is composed of mollusc shells deposited during the sea-level highstand that occurred during the second part of LIG. Our sample collection is therefore contemporaneous with the second part of the LIG, and is dated between ≈125 and ≈119-116 ky BP.

(ii) From 30 mollusc shell $\delta^{18}O$ values, SST comprised between 20.4±1.3°C and 22.2±1.2°C is estimated during the LIG record in the eastern Canary marine sedimentary sequences. Two mollusc shells, sampled from La Santa and at Matas Blancas in order to obtain ontogenetic profiles, provide a seasonal SST amplitude comprised between about 3.5°C and 6°C, similar to that of the present. The $\delta^{13}C$ variations recorded within one of these two mollusc shells, reflecting those of seawater DIC, are correlated with the SST and indicate seasonal variations in the intensity of the upwelling off the African coast similar to those of the present.

(iii) According to the modern SST documented in the eastern part of the Canary archipelago and the warming gradient established in this zone, we deduce an average SST value of about 19.4±0.1°C during the pre-industrial times. This conclusion enables us to propose a SST anomaly ranging from +1.0±1.4°C to +2.8±1.3°C during the second half of the LIG with respect to pre-industrial times. This warming, which concerns only the second part of the LIG, is in principle weaker than that of the first part of the interglacial (≈129 ka to

≈125 ka), where the insolation was maximum and greater than in the Holocene. It therefore indicates a lower value of the temperature anomaly for the LIG (≈129 ka to ≈116 ka).

(iv) This positive anomaly is consistent with the composition of the faunal species recorded in the marine highstand deposit with a warm extra-limital southern species (*Persististrombus latus* or *Strombus bubonius*), typical of warm sea water, which shows that at the time of the LIG marine sediment deposits it was warmer than in the present interglacial, as already documented by Muhs et al. (2014). In fact, the SST recorded by the specimens of *Persististrombus latus* is definitely higher (≈+1.2°C) than that recorded by all 30 mollusc shells. The co-occurrence in the deposit of cooler species, nowadays present in the Canary Islands, illustrates the SST cooling that set in at the end of the LIG.

(v) This positive anomaly is also consistent with a global mean surface temperature during the LIG that was warmer than in the Holocene (a warming that we estimate to be ≈+2°C in the first part of the LIG (≈130 ka BP), followed by ≈+1°C in the second part (≈126 to ≈119 ky BP). By contrast, it does not accommodate with the zonal negative anomaly of reconstructed SST (cooler temperature) at low latitudes in the North Atlantic (Hoffman et al., 2017). The positive anomaly is nonetheless fully consistent with all the other existing regional reconstructions (Sicre et al., 2000; Matsuzaki et al., 2011; Castañeda et al., 2009; Muhs et al., 2014; Montesinos et al., 2014), as well as with the regional simulations of air temperature (Pedersen et al., 2016). This finding calls into question the reconstructed zonal cooling at low latitude in the North Atlantic proposed by Hoffman et al. (2017) as well as data in other studies that may be based on this work (e.g., Fisher et al., 2018).

(vi) We interpret the positive SST anomaly as resulting principally from warming of the descending branch of the North Atlantic Gyre (Canary current) due to the excess summer insolation during the LIG with respect to the Holocene and, to a lesser degree, from a

weakening of the upwelling off the African coast. As the Canary current is part of the North Atlantic Gyre, this implies a warming that extended over the whole of the gyre.

Acknowledgements – The authors thank Erik Geissler, Michel Fontugne and Pascale Braconnot for helpful discussions on this manuscript. We are also deeply grateful to the reviewers of this publication for their relevant remarks. This study was funded by the Centre National de la Recherche Scientifique and the Institut Universitaire de France (CL).

References:

Abrantes, F., 1991. Variability of upwelling off NW Africa during the latest Quaternary: diatom evidence. *Paleoceanography* 6(4)**,** 431-460. https://doi.org/10.1029/91PA00049.

Adkins, J., deMenocal P., Eshel, G., 2006. The ‘‘African humid period’’ and the record of marine upwelling from excess ^{230}Th in Ocean Drilling Program Hole 658C. Paleoceanography 21, PA4203. https://doi:10.1029/2005PA001200.

Arbuszewski, J., deMenocal, P., Cléroux, C., Bradtmiller, L., Mix, A., 2013. Meridional shifts of the Atlantic intertropical convergence zone since the Last Glacial Maximum. Nature Geoscience 6, 959-962. https://doi:10.1038/NGEO1961.

Arístegui, J., Barton E., Álvarez-Salgado X., Santos A. M., Figueiras F., Kifani S., Hernández-León S., Mason E., Machú E., Demarcq H., 2009. Sub-regional ecosystem variability in the Canary Current upwelling. Progress in Oceanography 83, 33-48.

Armstrong, E. M. and Vazquez-Cuervo, J., 2001. A new global satellite-based sea surface temperature climatology. Geophys. Res. Letters 28, 22, 4199-4202. https://doi:10.1029/2001GL013316.

Bemis, B. E., Spero, H. J., 1998. Reevaluation of the oxygen isotopic composition of planktonic foraminifera: experimental results and revised paleotemperature equations,

Paleoceanography 13, 150-160.

Berger, A., 1988. Milankovitch theory and climate, Reviews of Geophysics 26, 624–657.

Blanchon, P., Eisenhauer, A., Fietzke, J., Liebetrau, V., 2009. Rapid sea-level rise and reef back-stepping at the close of the last interglacial highstand. Nature 458, 881–884.

Borges, R., Hernández-Guerra, A., Nykjaer, L., 2004. Analysis of sea surface temperature time series of the south-eastern North Atlantic, Intern. J. of Remote Sensing 25, 869-891. https://doi10.1080/0143116031000082442.

Bourget, E., Brock, V., 1990. Short-term shell growth in bivalves: individual, regional, and age-related variations in the rhythym of deposition of *Cerastoderma* (= *Cardium*) edule. Marine Biology 106, 103-108.

Brewer, S., Guiot, J., Sanchez-Goni, M. F., Klotz, S., 2008. The climate in Europe during the Eemian: a multi-method approach using pollen data. Quaternary Sc. Rev. 27, 2303–2315.

CAPE-Last Interglacial Project Members, 2006. Last Interglacial Arctic warmth confirms polar amplification of climate change. Quaternary Sc. Rev. 25, 1383-1400. https://doi.org/10.1016/j.quascirev.2006.01.033.

Capron, E., Govin, A., Stone, E., Masson-Delmotte, V., Mulitza, S., Otto-Bliesner, B., Rasmussen, T., Sime, L., Waelbroeck, C., Wolff, E., 2014. Temporal and spatial structure of multi-millennial temperature changes at high latitudes during the Las Interglacial. Quaternary Sc. Rev. 103, 116-133.

Capron, E., Govin, A., Stone, E.J., 2015. A new Last Interglacial temperature data synthesis as an improved benchmark for climate modeling. PAGES Magazine 23, 1, 4-5.

Capron, E., Govin, A., Stone, E. J., 2017a. Recent advances on the dynamical representation and our understanding of the warmer than present last interglacial climate. Quaternaire 28, 2, 185-193.

Capron, E., Govin, A., Feng, R., Otto-Bliesner, B.L., Wolff, E.W., 2017b. Critical evaluation

of climate syntheses to benchmark CMIP6/PMIP4 127 ka Last Interglacial simulations in the high-latitude regions. Quaternary Sc. Rev. 168, 137-150.

Carracedo, J. C., Pérez Torrado, F. J., Ancochea, E., Meco, J., Hernán, F., Cubas, C. R., Casillas, R., Rodríguez Badiola, E., Ahijado, A., 2002. Cenozoic volcanism II: the Canary Island, in: Gibbons, W., Moreno, T. (Eds.), The Geology of Spain. The Geological Society, London, pp.439-472.

Castañeda, I., Mulitza, S., Schefuß, E., Lopes dos Santos, R., Sinninghe Damsté, J., Schouten, S., 2009. Wet phases in the Sahara/Sahel rergion and human migration patterns in North Africa. PNAS 106, 20159-20163. https://doi:10.1073/pnas.0905771106.

Chambers, J.M., and Hastie, T., 1992. Statistical models in S, Chapman and Hall/CRC (Eds.), New York, 624 pp.

Charrette, M.A., and Smith, W.H., 2010. The volume of Earth's ocean. Oceanography 23, 112-114.

Chylek, P., and Lohmann, U., 2008. Aerosol radiative forcing and climate sensitivity deduced from the Last Glacial Maximum to Holocene transition. Geophys. Res. Letters 35, L04804. https://doi:10.1029/2007GL032759.

Clauzel, T., Maréchal, C., Fourel, F., Barral, A., Amiot, R., Betancort, J-F., Lomoschitz, A., Meco, J., Lécuyer, C., 2019. Reconstruction of sea-surface temperatures in the Canary Islands during Marine Isotope Stage 11. Quaternary Research 1-15. https://doi:10.1017/qua.2019.65.

CLIMAP Project members, 1984. The Last Interglacial Ocean. Quaternary Research 21, 123-224.

Collins, J., Prange, M., Caley, T., Gimeno, L., Beckmann, B., Mulitza, S., Skonieczny, C., Roche, D., Schefuß, E., 2017. Rapid termination of the African Humid Period triggered by

northern high-latitude cooling. Nature communications 8, 1372, 1-11. https://doi:10.1038/s41467-017-01454-y.

Conkright, M.E., Locarnini, R. A., Garcia, H.E., O'Brien, T.D., Boyer, T.P., Stephens, C., Antonov, J.I., 2002. World Ocean Atlas 2001: Objective Analyses, Data Statistics, and Figures, CD-ROM Documentation. National Oceanographic Data Center, Silver Spring, MD, pp. 17.

Coplen, T.B., Kendall, C., Hopple, J., 1983. Comparison of stable isotope reference samples, Nature 302, 236-238.

Cornu, S., Pitzold, J., Bard, E., Meco, J., Cuerda-Barcelo, J., 1993. Paleotemperature of the last interglacial period based on δ ^{18}O of *Strombus bubonius* from the western Mediterranean Sea. Paleogeography, Palaeoclimatology, Palaeoecology 103, 1-20.

Cosel, R. von, Gofas, S., 2019. Marine Bivalves of Tropical West Africa from Rio de Oro to southern Angola. Publications scientifiques du Muséum, Paris, IRD Marseille, 1104 pp.

Cuerda, J., 1987. Moluscos marinos y salobres del Pleistoceno balear. Caja de Baleares "Sa Nostra" Palma de Mallorca. ISBN 84-7535-110-7, 471 pp.

Darfeuil, S., Ménot, G., Giraud, X., Rostek, F., Tachikawa, K., Garcia, M., Bard, E., 2016. Sea surface temperature reconstructions over the last 70 kyr off Portugal: Biomarker data and regional modeling. Paleoceanography 31. https://doi:10.1002/2015PA002831.

deCastro, M., Gomez-Gesteira, M., Costoya, X., Santos, F., 2014. Upwelling influence on the number of extreme hot SST days along the Canary upwelling ecosystem. J. Geophys. Res. Oceans, 119. https://doi:10.1002/ 2013JC009745.

deMenocal, P., Ortiz, J., Guilderson, T., Adkins, J., Sarnthein, M., Baker, L., Yarusinsky, M., 2000. Abrupt onset and termination of the African Humid Period: rapid climate responses to gradual insolation forcing. Quaternary Sc. Rev. 19, 347-361.

Dome Fuji Ice Core Project Members, 2017. State dependence of climatic instability over the past 720,000 years from Antarctic ice cores and climate modeling. Sci. Adv. 3 : e1600446. https://doi: 10.1126/sciadv.1600446.

Dutton, A., Carlson, A., Long, A., Milne, G., Clark, P., DeConto, R., Horton, B. P., Rahmstorf, S., Raymo, M., 2015a. Sea-level rise due to polar ice-sheet mass loss during past warm periods. Science 349, 6244.

Dutton, A., Webster, J., Zwartz, D., Lambeck, K., Wohlfarth, B., 2015b. Tropical tales of polar ice: evidence of Last Interglacial polar ice sheet retreat recorded by fossil reefs of the granitic Seychelles islands. Quaternary Sc. Rev. 107, 182-196.

Eisma, D., 1965. Shell-characteristics of Cardium edule L. as indicators of salinity. Netherlands Journal of Sea Research 2 (4), 493-540.

Elderfield, H., Ferretti, P., Greaves, M., Crowhurst, S. J., Mc- Cave, I. N., Hodell, D. A., Piotrowski, A. M., 2012. Evolution of ocean temperature and ice volume through the Mid-Pleistocene Climate Transition. Science 337, 704–709.

Fischer, H., Meissner, K., Mix, A., Abram, N., Austermann, J., Brovkin, V., Capron, E., Colombaroli, D., Daniau, A-L., Dyez, K., Felis, T., Finkelstein, S., Jaccard, S., McClymont, E., Rovere, A., Sutter, J., Wolff, E., Affolter, S., Bakker, P., Ballesteros-Cánovas, J., Barbante, C., Caley, T., Carlson, A., Churakova (Sidorova), O., Cortese, G., Cumming, B., Davis,B., de Vernal, A., Emile-Geay, J., Fritz, S., Gierz, P., Gottschalk, J., Holloway, M., Joos, F., Kucera, M., Loutre, M-F., Lunt, D., Marcisz, K., Marlon, J., Martinez, P., Masson-Delmotte, V., Nehrbass-Ahles, C., Otto-Bliesner, B., Raible, C., Risebrobakken, B., Sánchez Goñi, M., Saleem Arrigo, J., Sarnthein, M., Sjolte, J., Stocker, T., Velasquez Alvárez, P., Tinner, W., Valdes, P., Vogel, H., Wanner, H., Yan, Q., Yu, Z., Ziegler, M., Zhou, L., 2018. Palaeoclimate constraints on the impact of 2°C anthropogenic

warming and beyond. Nature Geoscience 11, 474-485. https://doi:10.1038/s41561-018-0146-0.

Frank, P.W., 1969. Growth rates and longevity of some gastropod mollusk°Cs on the coral reef at Heron Island. Oecologia, 2, 2, 232-250.

Freudenthal, T., Meggers, H., Henderiks, J., Kuhlmann, H., Moreno, A., Wefer, G., 2002. Upwelling intensity and filament activity off Morocco during the last 250,000 years. Deep-Sea Research II, 49, 3655–3674.

Füllenbach, C., Schöne, B., Mertz-Kraus, R., 2015. Strontium/lithium ratio in aragonitic shells of *Cerastoderma edule* (Bivalvia) – A new potential temperature proxy for brackish environments. Chemical Geology 417, 341-355.

Gillet, P., Gérard, Y., Willaime, C., 1987. The calcite-aragonite transition : mechanism and microstructures induced by the transformation stresses and strain. Bulletin de Minéralogie 110, 481-496.

Gillet, P., Biellmann, C., Reynard, B., McMillan, P., 1993. Raman spectroscopic studies of carbonates Part I: High-pressure and high-temperature behaviour of calcite, magnesite, dolomite and aragonite. Physics and Chemistry of Minerals 20, 1–18.

Goelzer, H., Huybrechts, P., Loutre, M.-F., Fichefet, T. 2016. Last Interglacial climate and sea-level evolution from a coupled ice sheet–climate model. Climate of the Past 12, 2195-2213.

Gómez-Letona, M., Ramos, A. G., Coca, J., Arístegui, J. (2017) Trends in Primary Production in the Canary Current Upwelling System — A Regional Perspective Comparing Remote Sensing Models Frontiers. Marine Science 4, Article 370. https://doi.org/10.3389/fmars.2017.00370.

Grossman, E. L., Ku, T.-L., 1986. Oxygen and carbon isotope fractionation in biogenic aragonite : temperature effect. Chemical Geology 59, 59-74.

Hansen, J., Sato, M., Kharecha, P., Beerling, D., Berner, R., Masson-Delmotte, V., Pagani, M., Raymo, M., Royer, D., Zachos, J., 2008. Target atmospheric CO_2: where should humanity aim ? The Open Atmospheric Science Journal 2, 217-231.

Hansen, J., Sato, M., Russell, G., Kharecha, P. 2013. Climate sensitivity, sea level and atmospheric carbon dioxide. Phil. Trans. Roy. Soc. A 371, 20120294. https://doi.org/10.1098/rsta.2012.0294.

Henderiks, J., Freudenthal, T., Meggers, H., Nave, S., 2002. Glacial–interglacial variability of particle accumulation in the Canary Basin: a time-slice approach. Deep-Sea Research II 49, 3675–3705.

Hessler, I., Harrison, S., Kucera, M., Waelbroeck, C., Chen, M-T., Anderson, C., de Vernal, A., Fréchette, B., Cloke-Hayes, A., Leduc, G., Londeix, L., 2014. Implication of methodological uncertaintiesfor mid-Holocene sea surface temperature reconstructions. Climate of the Past 10, 2237-2252. https://doi:10.5194/cp-10-2237-2014.

Hoffman, J. S., Clark, P. U., Parnell, A. C., He, F. 2017. Regional and global sea-surface temperatures during the last interglaciation. Science 355, 276–279.

Hut, G., 1987. Consultant's group meeting on stable isotope reference samples for geochemical and hydrological investigations. International Energy Atomic Agency, pp. 42.

IPCC, 2013. Climate Change 2013: The Physical Science Basis, Contribution of working group 1 to the fifth Assessment Report of the Intergouvernmental Panel on Climat Change, in: Stocker, T. F., Qin, D., Plattner, G.-K., Tignor, M., Allen, S. K., Boschung, J., Nauels, A., Xia, Y., Bex, V., Midgley, P. M. (Eds.). Cambridge University Press, Cambridge and New York.

Jouzel, J., Masson-Delmotte, V., Cattani, O., Dreyfus, G., Falourd, S., Hoffmann, G., Minster, B., Nouet, J., Barnola, J.M., Chappellaz, J., Fischer, H., Gallet, J.C., Johnsen, S., Leuenberger, M., Loulergue, L., Luethi, D., Oerter, H., Parrenin, F., Raisbeck, G.,

Raynaud, D., Schilt, A., Schwander, J., Selmo, E., Souchez, R., Spahni, R., Stauffer, B., Steffensen, J.P., Stenni, B., Stocker, T.F., Tison, J.L., Werner, M., Wolff, E.W. 2007. Orbital and millennial Antarctic climate variability over the past 800,000 years. Science 317, 793-796.

Kaspar, F., Kühl, N., Cubasch, U., Litt, T. 2005. A model-data comparison of European temperatures in the Eemian interglacial. Geophys. Res. Letter 32, L11703. https://doi:10.1029/2005GL022456.

Killops, S., Killops, V., 2005. Introduction to Organic Geochemistry, Blackwell, Oxford.

Kim, S.T., O'Neil J.R., 1997. Equilibrium and nonequilibrium oxygen isotope effects in synthetic carbonates. Geochimica et Cosmochimica Acta 61, 16, 3461–3475.

Kim, S.T., Mucci, A., Taylor B.E., 2007a. Phosphoric acid fractionation factors for calcite and aragonite between 25 and 75°C: Revisited. Chemical Geology 246, 135–146.

Kim, S.T., O'Neil, J.R., Hillaire-Marcel, C., Mucci, A., 2007b. Oxygen isotope fractionation between synthetic aragonite and water: Influence of temperature and Mg^{2+} concentration, Geochimica et Cosmochimica Acta 71, 4704–4715.

Kopp, R. E., Simons, F. J., Mitrovica, J. X., Maloof, A. C., Oppenheimer, M., 2013. A probabilistic assessment sea level variations within the last interglacial stage. Geophys J. International. 193, 711–716.

Landais, A., Barkan, E., Luz, B., 2008. Record of d18O and 17o-excess in ice from Vostok Antarctica during the last 150,000 years. Geophys. Res. Letters 35, L02709. https://doi:10.1029/2007GL032096.

Lambeck, K., Rouby, H., Purcell, A., Sun, Y., Sambridge, M., 2014. Sea level and global ice volumes from the Last Glacial Maximum to the Holocene. Proc. Natl. Acad. Sci. 111, 15296–15303.

1267 Lécuyer, C., Atrops,F., Amiot,R., Angst, D., Daux,V., Flandrois, J.-P., Fourel,F., Rey, K.,
1268 Royer,A., Seris, M., Touzeau, A., Rousseau, D.-D., 2018. Tsunami sedimentary deposits of
1269 Crete records climate during the 'Minoan Warming Period' (≈3350 yr BP). The Holocene
1270 28, 6, 914–929.
1271 Lézine, A_M., Hély, C., Grenier, C., Braconnot, P., Krinner, G., 2011. Sahara and Sahel
1272 vulnerability to climate changes, lessons from Holocene hydrological data. Quaternary Sc.
1273 Rev. 30, 3001-3012.
1274 Lisiecki, L.E., and Raymo, M.E., 2005. A Pliocene-Pleistocene stack of 57 globally
1275 distributed benthic $\delta^{18}O$ records. Paleoceanography 20, 1, 1003.
1276 Luque, A., Martín, J. L., Dorta, P., Mayer, P. 2014. Temperature Trends on Gran Canaria
1277 (Canary Islands), an Example of Global Warming over the Subtropical Northeastern
1278 Atlantic. Atmospheric and Climate Sciences 4, 20-28.
1279 Mackensen, A., Hubberten, H.W., Bickert, T., Fischer, G., Filtterer, D.K., 1993. The $\delta^{13}C$ in
1280 benthic foraminifera tests of *Fontbotia wuellerstorfi* relative to the $\delta^{13}C$ of dissolved
1281 inorganic carbon in Southern Ocean deep Water: Implications for ocean circulation
1282 models. Paleoceanography 8, 587–610.
1283 Marcott, S. A., Shakun, J. D., Clark, P. U., Mix, A. C., 2013. A reconstruction of regional and
1284 global temperature for the past 11,300 years. Science 339, 6124, 1198-2001.
1285 https://doi.10.1126/science.1228026.
1286 Martín, J. L., J. L., Bethencourt, J., Cuevas-Agulló, E., 2012. Assessment of global warming
1287 on the island of Tenerife, Canary Islands (Spain), trends in minimum, maximum and mean
1288 temperatures since 1944. Climatic Change 114, 343–355.
1289 Maslin, M.A., and Swann, G.E., 2005. Isotopes in marine sediments, in: Isotopes in
1290 Palaeoenvironmental Research. Leng, M.J. (ed.), Springer, Dordrecht, The Netherlands,
1291 pp. 227–290.

Masson-Delmotte, V., Stenni, B., Pol, K., Braconnot, P., Cattani, O., Falourd, S., Kageyama, M., Jouzel, J., Landais, A., Minster, B., Barnola, J.M., Chappellaz, J., Krinner, G. Johnsen, S., Röthlisberger, R., Hansen, J., Mikolajewicz, U., Otto-Bliesner, B., 2010. EPICA Dome C record of glacial and interglacial intensities. Quaternary Sc. Rev. 29, 113–128.

Masson-Delmotte, V., Schulz, M., Abe-Ouchi, A., Beer, J., Ganopolski, J., González Rouco, J.F., Jansen, E., Lambeck, K., Luterbacher, J., Naish, T., Osborn, T., Otto-Bliesner, B., Quinn, T., Ramesh, R., Rojas, M., Shao, X., Timmermann, A., 2013. Information from paleoclimate archives, in: Stocker, T. F., Qin, D., Plattner, G.-K., Tignor, M., Allen, S. K., Boschung, J., Nauels, A., Xia, Y., Bex, V., Midgley, P. M. (Eds.), Climate Change 2013: The Physical Science Basis : Contribution of working group 1 to the fifth Assessment Report of the Intergouvernmental Panel on Climat Change. Cambridge University Press, Cambridge and New York, pp. 383-464.

Matsuzaki, K.M.R., Eynaud, F., Malaizé, B., Grousset, F.E., Tisserand, A., Rossignol, L., Charlier, K., Jullien, E., 2011. Paleoceanography of the Mauritanian margin during the last two climatic cycles : from planktonic foraminifera to African climate dynamics. Marine Micropaleontology 79, 67-79.

McKay, N., Overpeck, J., Otto-Bliesner, B., 2011. The role of ocean thermal expansion in Last Interglacial sea level rise. Geoph. Res. Letters 38, L14605. https://doi:10.1029/2011GL048280, 2011.

McManus, J. F**,** Oppo, D. W**,** Cullen J. L, **1999.** Stable carbon and oxygen isotope ratios of Cibicidoides wuellerstorfi in the 340 to 0 kyr section of ODP Site 162-980 in the subpolar North Atlantic. *PANGAEA*. https://doi.org/10.1594/PANGAEA.700818.

Meco, J., 1977. Paleontología de Canarias I: Los Strombus neógenos y cuaternarios del Atlántico euroafricano (taxonomía, biostratigrafía y paleoecología). Cabildo Insular de Gran Canaria, Madrid, 206 pp.

Meco, J., and Stearns, C. E., 1981. Emergent littoral deposits in the Eastern Canary Islands. Quaternary Research 15, 199-208.

Meco, J., Petit-maire, N., Reyss, J.-L., 1992. Le courant des Canaries pendant le stade isotopique 5 d'après la composition faunistique d'un haut niveau marin a Fuerteventura (28ºN). C. Rendu Académie Sc. Paris 314, 203-208.

Meco, J., Guillou, H., Carracedo, J-C., Lomoschitz, A., Ramos, A-J., Rodríguez-Yánez, J-J., 2002. The maximum warmings of the Pleistocene world climate recorded in the Canary Islands. Palaeogeography, Palaeoclimatology, Palaeoecology 185, 197-210.

Meco, J., Ballester, J., Betancort, J.-F., Cilleros, A., Scaillet, S., Guillou, H., Carracedo, J.-C., Lomoschitz, A., Petit-Maire, N., Ramos, A-J. G., Perera, N., Meco, J.-M., 2006. Paleoclimatologia del Neogeno en las Islas Canarias, Geliense, Pleistoceno y Holoceno, Ministerio de Medio Ambiente, Univ. de Las Palmas de Gran Canaria.

Meco, J., Ballester, J., Soler, E., Betancort, J-F., 2007. Los fósiles del Pleistoceno marino de Las Palmas (Gran Canaria) y de La Guirra (Fuerteventura). In Pons, G. X., i Vicens, D. (Edit.). Geomorfologia Litoral I Quaternari. Homenatge a Joan Cuerda Barceló. Monografies de la Societat d'Història Natural de les Balears 14, 37-48. ISBN 84-96376_13-3. Palma de Mallorca.

Meco, J., Muhs, D., Fontugne, M., Ramos, A., Lomoschitz, A., Patterson, D., 2011. Late Pliocene and Quaternary Eurasian locust infestations in the Canary Archipelago. Lethaia 44, 440-454.

Meco, J., Lomoschitz, A., Rodriguez, A., Ramos, A-J. G., Betancort, J.-F., Coca, J., 2018. Mid and Late Holocene sea level variations in the Canary Islands. Palaeogeography, Palaeoclimatology, Palaeoecology 507, 214–225.

Mélières, M.-A., Maréchal, C.N., 2015. Climate change: past, present and future, p. 181-190, Wiley Blackwell, Oxford, 391 pp.

Milankovitch, M., 1941. Kanon der Erdbestrahlung und Seine Anwendung auf das Eiszeitenproblem (Canon of Insolation and the Ice-age Problem).

Mittelstaedt, E. 1991. The ocean boundary along the African coast. Circulation and oceanographic properties at the sea surface. Progress in Oceanography 26, 307–455.

Montesinos, M., Ramos, A.J.G., Lomoschitz, A., Coca, J., Redondo, A., Betancort, J.-F., Meco, J., 2014. Extralimital Senegalese species during Marine Isotope Stages 5.5 and 11 in the Canary Islands (29° N): sea surface temperature estimates. Palaeogeography, Palaeoclimatology, Palaeoecology 410, 153–163.

Moreno, A., Nave, S., Kuhlmann, H., Canals, M., Targarona, J., Freudenthal, T., Abrantes, F., 2002. Productivity response in the Norht Canary Basin to climate changes during the last 250 000 yr: a multi-proxy approach. Earth Planet. Sci. Lett. 196, 147-159.

Moss, D. K., Ivany, L. C., Judd, E. J., Cummings, P. W., Bearden, C. E., Kim, W. J., Artruc E.G., Driscoll, J. R., 2016. Lifespan, growth rate, and body size across latitude in marine Bivalvia, with implications for Phanerozoic evolution. Proceedings of the Royal Society B: Biological Sciences 283, 1836, 20161364.

Muhs, D.R., Meco, J., Simmons, K.R., 2014. Uranium-series ages of corals, sea level history, and palaeozoogeography, Canary Islands, Spain: an exploratory study for two Quaternary interglacial periods. Palaeogeography, Palaeoclimatology, Palaeoecology 394, 99–118.

Navarro-Pérez, E., Barton, E.D., 2001.Seasonal and interannual variability of the Canary Current. Scientia Marina 65, Supp. 1, 205-213.

Nave, S., Freitas, P., Abrantes, F., 2001. Coastal upwelling in the Canary Island region : spatial variability reflected by the surface sediment diatom record. Marine Micropaleontology 42, 1-23.

Nave, S., Salgueiro, E., Abrantes, F., 2003. Siliceous sedimentary record of the last 280 kyr in the Canary basin (NW Africa). Marine Geology 196, 21-35.

Niclès, M., 1950. Mollusques testacés marins de la Côte occidentale d'Afrique. Lechevalier éd., Paris, 269 pp.

North Greenland Ice Core Project members, 2004. High-resolution record of Northern Hemisphere climate extending inot the Last Interglacial period. Nature, 2805. https://doi:10.1038/nature02805.

O'Leary, M., Hearty, P., Thompson, W., Raymo, M., Mitrovica, J., Webster, J., 2013. Ice sheet collapse following a prolonged period of stable sea level during the last interglacial. Nature Geoscience 6, 796-800.

Pardo, P.C., Padín, X.A., Gilcoto, M., Farina-Busto, L., Pérez, F.F., 2011.Evolution of upwelling systems coupled to the long-term variability in sea surface temperature and Ekman transport. Clim. Res. 48: 231–246.

Past Interglacials Working Group of PAGES, 2016. Interglacials of the last 800,000 years. Rev. Geophys. 54, 162–219. https://doi:10.1002/2015RG000482.

Pedersen, R., Langen, P., Vinther, B., 2017. The last interglacial climate: comparing direct and indirect impacts of insolation changes. Climate Dynamics 48, 3391-3407. https://doi:10.1007/s00382-016-3274-5.

Peeters, F., Brummera, G-J., Ganssen, G., 2002. The effect of upwelling on the distribution and stable isotope composition of *Globigerina bulloides* and *Globigerinoides ruber* (planktic foraminifera) in modern surface waters of the NW Arabian Sea. Global and Planetary Change 34, 269-291.

Richardson, C. A., Crips, D. J., Runham, N. W., 1980. Factors influencing shell growth In Cerastoderma edule. Proceedings of the Royal Society of London, B 210, 513-531.

Rognon, P., and Coude-Gaussen, G., 1996. Change in atmospheric and oceanic circulations at the latitude of the Canaries and Morocco between isotopic stages 2 and 1. Quaternaire 7, 4, 197-206.

Rohling, E.J., and Cooke, S., 1999. Stable oxygen and carbon isotopes in foraminiferal carbonate shells, in: Sen Gupta B.K. (Ed.), Modern Foraminifera. Kluwer Academic, Dordrecht, pp. 239–258.

Rohling, E.J., Grant, K., Bolshaw, M., Roberts, A. P., Siddall, M., Hemleben, Ch., Kucera, M., 2009. Antarctic temperature and global sea level closely coupled over the past five glacial cycles. Nature Geoscience 2, 500–504.

Rohling, E. J., Grant, K. M., Bolshaw, M., Roberts, A. P., Sid- dall, M., Hemleben, C., Kucera, M., Foster, G. L., Marino, G., Roberts, A. P., Tamisiea, M. E., Williams, F., 2014. Sea-level and deep-sea-temperature variability over the past 5.3 million years. Nature 508, 477–482.

Rolán, E., 2011. Moluscos y conchas marinas de Canarias, ConchBooks, Hackenheim and Rolán (Eds.), Vigo, 716 pp.

Roman-Roman, P., Romero, D., Torres-Ruiz, F., 2010. A diffusion process to model generalized von Bertalanffy growth patterns: Fitting to real data. Journal of Theoretical Biology 263, 59–69.

Rossignol-Strick, M., 1985. Mediterranean quaternary sapropels : an immediate response of the African monsoon to variation of insolation. Paleogeography, Paleoclimatology, Paleoecology 49, 237-261.

Sadler, J., Carré, M., Azzoug, M., Schauer, A. J., Ledesma, J., Cardenas, F., Chase, B. M., Bentaleb, I., Muller, S. D., Mandeng, M., Rohling E. J., Sachs, J. P., 2012. Reconstructing past upwelling intensity and the seasonal dynamics of primary productivity along the

Peruvian coastline from mollusk shell stable isotopes. Geochemistry, Geophysics, Geosystems 13. https://doi:10.1029/2011GC003595.

Santos, F., deCastro, M., Gómez-Gesteira, M., Álvarez, I., 2012. Differences in coastal and oceanic SST warming rates along the Canary upwelling ecosystem from 1982 to 2010. Continental Shelf Research 47, 1-6.

Sarnthein, M., Erlenkeuser, H., Zahn, R., 1982. Termination I : The response of continental climate in the subtropics as recorded in deep-sea sediments. Bull. Inst. Geol. Bassin Aquitaine 31, 393-407.

Sarnthein, M, Winn, K, Duplessy, J-C, Fontugne, M.R., 1988. Global variations of surface ocean productivity in low and mid latitudes: Influence on CO_2 reservoirs of the deep ocean and atmosphere during the last 21,000 years. Paleoceanography and Paleoclimatology 3, 3, 361-399.

Shackleton, N., 1987. Oxygen isotopes, ice volume and sea level. Quaternary Sc. Rev. 6, 3-4, 183–190.

Shackleton, N., Hall, M., Vincent, E., 2000. Stable carbon and oxygen isotope ratios of foraminifera from sediments of the Iberian margin. *PANGAEA*. doi.org/10.1594/PANGAEA.700954.

Shakun, J., 2015. 800-kyr record of global surface ocean $\delta^{18}O$ and implications for ice volume-temperature coupling. Earth Planet. Sci. Lett. 426, 58–68.

Shanahan, T., McKay, N., Hughen, K., Overpeck, ATJ., Otto-Bliesner, B., Heil, C., King, J., Scholz, C., Peck, J., 2015. The time-transgressive termination of the African Humid Period. Nature Geoscience 8, 140-144. https://doi:10.1038/NGEO2329.

Sicre, M-A., Ternois, Y., Paterne, M., Boireau, A., Beaufort, L., Martinez, P., Bertrand, P. 2000. Biomarker stratigraphic records over the last 150 kyears off the NW African coast at 25°N. Organic Geochemistry 31, 577-588.

Snyder, C. W., 2016. Evolution of global temperature over the past two million years. Nature 538, 7624, 226-228. https://doi: 10.1038/nature19798.

Sosdian, S., and Rosenthal, Y., 2009. Deep-Sea temperature and ice volume changes across the Pliocene-Pleistocene climate transitions. Science 325, 306–310.

Sousa, M., Alvarez, I., deCastro, M., Gomez-Gesteira, M., Dias, J., 2017. Seasonality of coastal upwelling trends under future warming scenarios along the southern limit of the canary upwelling system. Progress in Oceanography 153, 16-23.

Spratt, R. M., and Lisiecki, E., 2016. A Late Pleistocene sea level stack. Clim. Past 12, 1079–1092.

Stark, J.D., Donlon, C.J., Martin M.J., McCulloch, M.E., 2007. OSTIA: An operational, high resolution, real time, global sea surface temperature analysis system. In: Oceans ’07 IEEE Aberdee, Conference Proceedings. Marine Challenges: Coastline ot Deep Sea. Aberdeen, Scotland.

Thompson, W., Curran, H., Wilson, M., White, B., 2011. Sea-level oscillations during the last interglacial highstand recorded by Bahamas corals. Nature Geoscience 4, 684-687.

Turney, C. S., Jones, R. T., 2010. Does the Agulhas Current amplify global temperatures during super-interglacials ? J. Quaternary Sci. 25, 6, 839–843.

Unvros, J., Sharma, S., Mackenzie, F., 1991. Characterization of some biogenic carbonates with Raman spectroscopy. American Mineralogist 76, 641–646.

Waelbroeck, C., Labeyrie, L., Michela, E., Duplessy, J.C., McManus, J.F., Lambeck, K., Balbona, E., Labracherie, M., 2002. Sea-level and deep water temperature changes derived from benthic foraminifera isotopic records. Quaternary Sc. Rev. 21, 295–305.

Wang, P., Wang, B., Kiefer, T., 2009. Global monsoon in observations, simulations and geological records. PAGES News 17, 2, 82-83.

Zazo, C., Goy, J.L., Hillaire–Marcel, Cl., Gillot, P.Y., Soler, V., González, J.A., Dabrio, C.J., Ghaleb, B., 2002. Raised marine sequences of Lanzarote and Fuerteventura revisited - a reappraisal of relative sea-level changes and vertical movements in the eastern Canary Island during the Quaternary. Quaternary Sc. Rev. 21, 2019–2046.

Tables captions

Table 1 : Present sea surface temperature (SST in °C) in the eastern Canary Islands. (*) Values and standard errors estimated from color codes indicated on the figures.

Table 2: Period of sea-level (SL) highstand(s) during the LIG, together with the sea-level anomaly relative to the modern period.

Table 3 : Different studies reconstructing the SST during the LIG in the northeast tropical Atlantic.

Figure captions

Figure 1: (a) Location of the Canary Islands and of the Canary Current (blue arrows). (b) Map of eastern Canary Islands and sites of the marine deposits from the Last Interglacial period (red circles) including the LIG marine terrace deposits studied here at La Santa, Lanzarote, and Matas Blancas, Fuerteventura (yellow squares). Sites of coastal water samplings in the eastern Canary Islands are indicated by blue stars (Clauzel el al., 2019). LPG = Las Palmas de Gran Canaria, MB = Matas Blancas, LP = Las Playitas, LG = La Guirra, LS = La Santa, PP = Punta Penedo, M = Matagorda, NGC = North Gran Canaria, NFV = North Fuerteventura, WLZ = West Lanzarote.

Figure 2 : (a) Stratigraphy of cliff sections at Punta Penedo site, a few kilometers north of the site at La Santa, Lanzarote, studied here, showing the most complete section in the area (adapted from Meco et al., 2006). The sedimentary deposits are characterized by a succession of four distinct climatic phases: (i) calcareous dune deposits, (ii) paleosols (with locust egg pods), (iii) marine sediments, and (iv) pedogenic calcretes (see text). (b) Marine deposits at the studied site at Matas Blancas (Fuerteventura) (Muhs et al., 2014) with well-preserved fossil specimens of *Persististrombus latus* (*Strombus bubonius)*.

Figure 3 : (a) Annual mean sea surface temperature (SST in °C) in the North Atlantic Ocean from Pathfinder satellite (adapted from Darfeuil et al., 2016, data from Armstrong and Vazquez-Cuervo, 2001). The surface circulation patterns are indicated by black arrows. AzC = Azores Current, CC = Canary Current, PC = Portugal Current. (b) SST (°C) in the northeast tropical Atlantic Ocean on 25 July 2007 from OSTIA satellite (adapted from Arístegui et al., 2009, data from Stark et al., 2007). Studies reporting a LIG SST record and discussed in the present work are indicated by filled circles (sediment cores) and by empty circles (marine deposits). Black arrows correspond to Trade Winds (from Nave et al., 2003).

Figure 4: Photographs of a selection of shells of the 6 studied molluscan species : gastropods (a) *Cerithium vulgatum*, (b) *Stramonita haemastoma*, (c) *Luria Lurida*, (d) *Persististrombus latus (Strombus bubonius)* and bivalves (e) *Loripes lacteus,* (f) *Cardium edule (Cerastoderma edule)*. The length of a rectangle corresponds to 1 cm.

Figure 5: Modern geographical distribution of the mollusc species studied in the la Santa, Lanzarote, and Matas Blancas, Fuerteventura, marine LIG deposits of the Canary Islands,

from south (red) to north (blue) of the archipelago (orange). The solid lines indicate the observed presence of the molluscs, the dashed lines their presumed presence.

Figure 6: (a) Sediments in the Canary Islands from the paleosols, corresponding to the African Humid Period, and from the marine deposits during the Holocene (Meco et al., 2011); (b) Antarctic temperature anomaly records (°C) from δD measurements of the ice at EPICA Dome C during the last 30 ky and (c) in the period 140-100 ky BP (Jouzel et al., 2007); (d) Sea-level variation (m) reconstructed from far-field coral and sediment data during the last 30 ky (grey circles) (Lambeck et al., 2014); (e) Sea-level variation (m) in the period 140-100 ky BP, reconstructed from combined field observations and glacial isostatic adjustment modeling (orange bar) (Dutton et al., 2015a) and from benthic foraminifera oxygen isotope ratios (grey curves) (adapted from Waelbroeck et al., 2002).The red and blue vertical lines correspond to the moment when the maximum temperature and the maximum sea-level, respectively, were reached during the interglacials. The green arrows indicate the lapse of several thousand years between these two moments. The blue dashed vertical line indicating the beginning of the highstand and the blue dashed curves describing the sea-level correspond to our interpretation (see text).

Figure 7: Raman spectra of selected mollusc shells sampled from La Santa, Lanzarote ((a) gastropod *Cerithium vulgatum* LAS-BULK-3 and (b) bivalve *Cardium edule (Cerastoderma edule)* LAS-INCR-14) and from Matas Blancas, Fuerteventura ((c) gastropod *Persististrombus latus (Strombus bubonius)* MAB-BULK-1 and (d) bivalve *Stramonita haemastoma* MAB-INCR-4). All these shells are made of aragonite that is characterized by the presence of relative intense peaks in the 150–250 cm^{-1} range, and a splitting of the

carbonate group bending mode yielding a doublet at 700–701 cm^{-1}. The peak located at 1080–1082 cm^{-1} is characteristic of the carbonate group stretching mode.

Figure 8: $\delta^{18}O$ (‰ V-PDB) of aragonitic shell increments of *Cardium edule* sampled from La Santa, Lanzarote, as a function of the distance from the umbo (cm) along the growth direction.

Figure 9: $\delta^{13}C$ (‰ V-PDB) as a function of $\delta^{18}O$ (‰ V-PDB) of aragonitic shell increments of (a) *Cardium edule* sampled from La Santa, Lanzarote and (b) *Stramonita haemastoma* sampled from Matas Blancas, Fuerteventura. (a) The regression line (red) is shown with its regression equation and coefficient ($R^2 = 0.51$).

Figure 10: Frequency histogram of reconstructed LIG SST from bulk mollusc shells sampled from La Santa, Lanzarote, and Matas Blancas, Fuerteventura, according to Equation (1) determined by Grossman and Ku (1986) (blue, on the left-hand side) and to Equation (2) determined by Kim et al. (2007b) (green, on the right-hand side).

Figure 11: Reconstructed LIG SST during the ontogenetic evolution of *Stramonita haemastoma* (Matas Blancas, Fuerteventura) according to Equation (1) determined by Grossman and Ku (1986) (blue) and to Equation (2) determined by Kim et al. (2007b) (green). The total length to apex is 16.0 cm.

Figure 12: Reconstructed LIG SST during the ontogenetic evolution of *Cardium edule* or *Cerastoderma edule* (La Santa, Lanzarote) according to Equation (1) determined by

Grossman and Ku (1986) (blue) and to Equation (2) determined by Kim et al. (2007b) (green). The total length to umbo is 4.5 cm.

Figure 13 : SST (°C) anomalies in the northeast tropical Atlantic relative (a) to core top values and (b) to the pre-industrial times. (1): Sicre et al. (2000), (2): Matsuzaki et al. (2011), (3): Castañeda et al. (2009), (1*) (2*) (3*): The same studies with SST anomalies estimated for the pre-industrial times (see text), (4): This study, (5): Adapted from Montesinos et al. (2014) (see text), (7), (8), (9): Hoffman et al. (2017) with cores GIK15637-1 (7), M12392-1 (8), V22-196 (9). See Figure 3(b) for the sites location.

Supplementary material captions:

Table captions

Table S1: Oxygen and carbon isotope compositions of bulk marine mollusc shells, listed together with calculated sea surface temperatures (SST) according to the oxygen isotope fractionation equations of Grossman and Ku (1986) (Eq.(1)) and Kim et al. (2007b) (Eq.(2)). Samples collected from La Santa, Lanzarote (LAS-BULK-1 to LAS-BULK-27) and from Matas Blancas, Fuerteventura (MAB-BULK-1 to MAB-BULK-3).

Table S2: Oxygen and carbon isotope compositions of marine mollusc shell increments and calculated sea surface temperatures (SST) according to the oxygen isotope fractionation equations of Grossman and Ku (1986) (Eq.(1)) and Kim et al. (2007b) (Eq.(2)). The *Cardium edule* specimen was collected from La Santa, Lanzarote (LAS-INCR-1 to LAS-

INCR-16) and the *Stramonita haemastoma* specimen from Matas Blancas, Fuerteventura (MAB-INCR-1 to MAB-INCR-29). Note: MAB-INCR-20 is missing.

Figure captions

Figure S1: (a) Cross-section of a bivalve shell showing the growth direction of the shell from the umbo (adapted from Füllenbach et al., 2015). (b) Photomicrograph of the bivalve *Cardium edule (Cerastoderma edule)* with the incremental samplings carried out along the growth axis (drilling holes). (c) Diagram of a gastropod shell showing the growth spiral of the shell from the apex (frontal view). (d) Photomicrograph of the gastropod *Stramonita haemastoma* with the incremental samplings, represented by grey circles, made along the growth spiral. The length of a rectangle corresponds to 1 cm.

Figure S2: $\delta^{13}C$ (‰ V-PDB) as a function of reconstructed SST (°C) of aragonitic shell increments of *Cardium edule* sampled from La Santa, Lanzarote. The regression line (red) is shown with its regression equation and coefficient ($R^2 = 0.51$). High SSTs occur in summer (Meco et al., 2018) a season where the upwelling activity is the strongest (Pardo et al., 2011; Navarro-Pérez and Barton, 2001; Mittelstaedt, 1991).

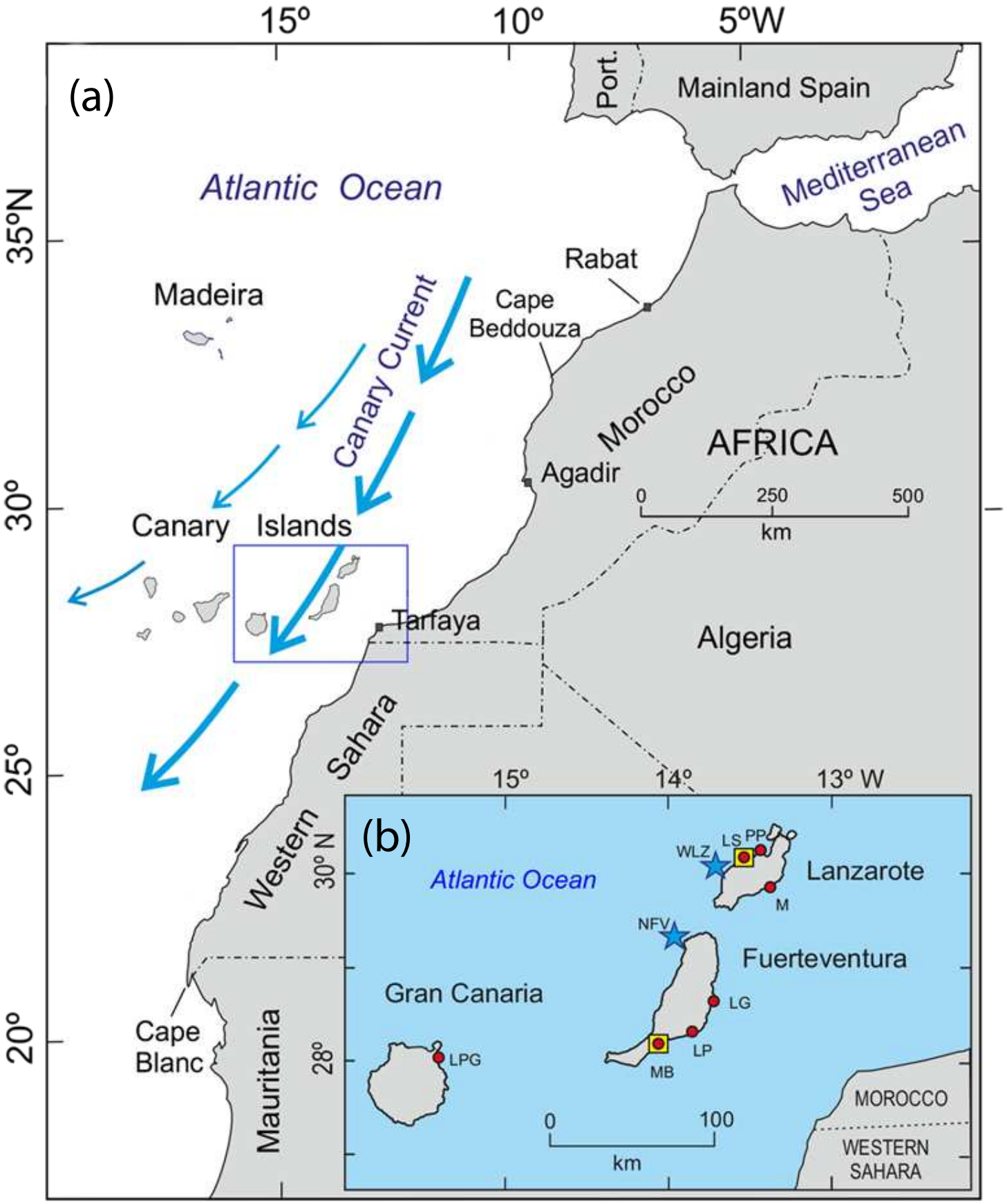
(a)
15°
10°
5°W
35°N
30°
25°
20°
Port.
Mainland Spain
Atlantic Ocean
Mediterranean Sea
Rabat
Madeira
Cape Beddouza
Canary Current
Morocco
AFRICA
Agadir
0 250 500
km
Canary Islands
Tarfaya
Algeria
Sahara
Western
Cape Blanc
Mauritania
(b)
15°
14°
13° W
30° N
28°
Atlantic Ocean
WLZ
LS
PP
Lanzarote
M
NFV
Fuerteventura
Gran Canaria
LG
LP
MB
LPG
0 100
km
MOROCCO
WESTERN SAHARA

(a) Punta Penedo (close to La Santa)

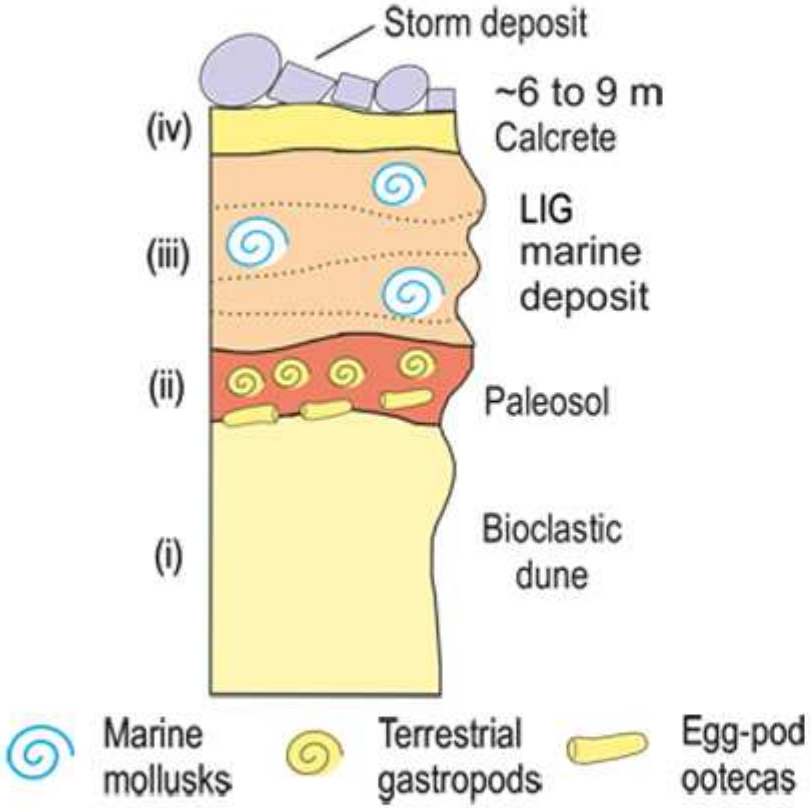

(b) Matas Blancas

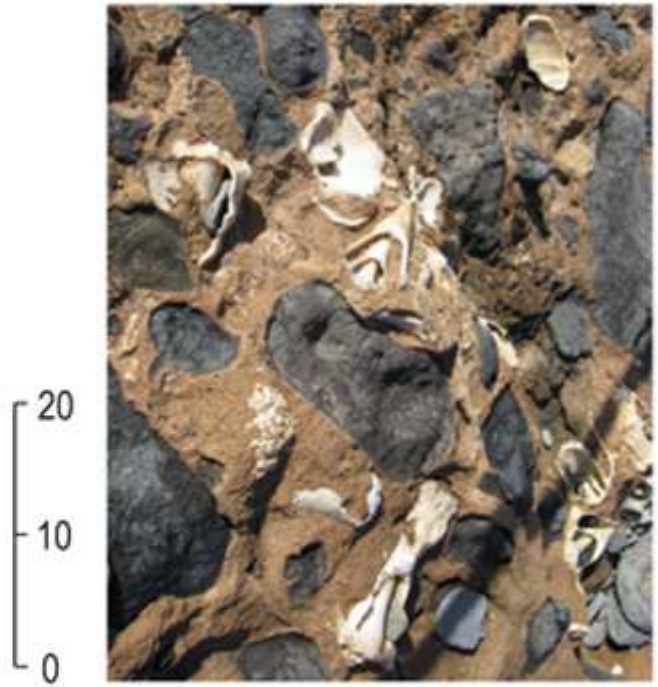

~1 m above present m.s.l.

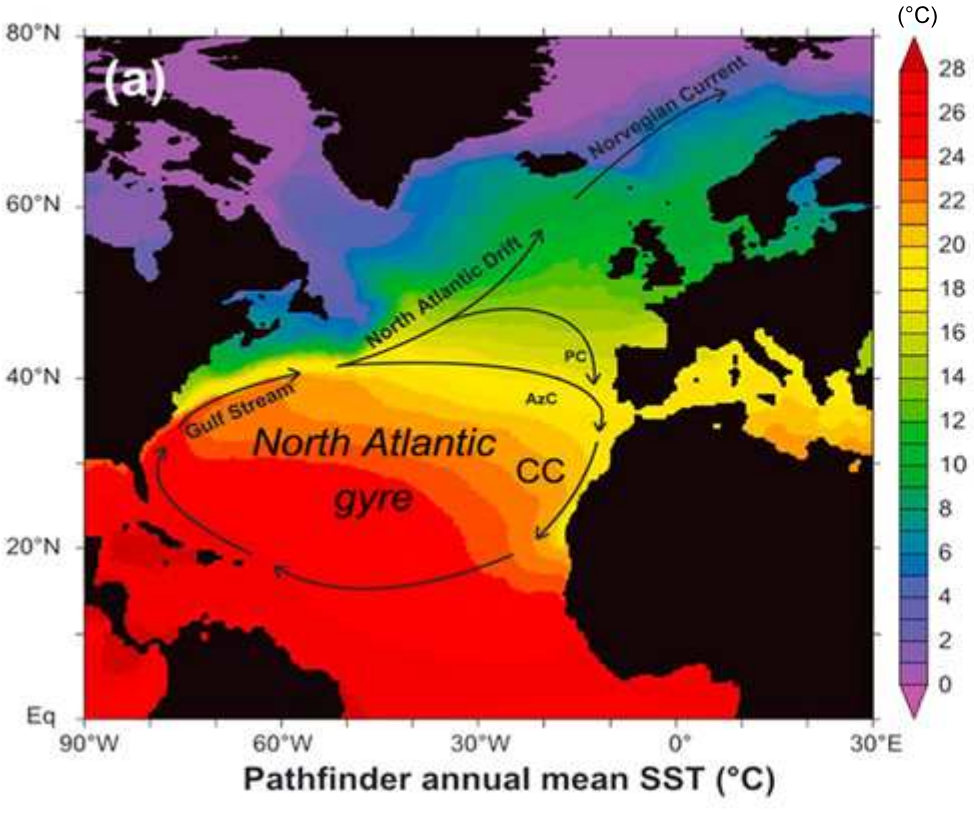

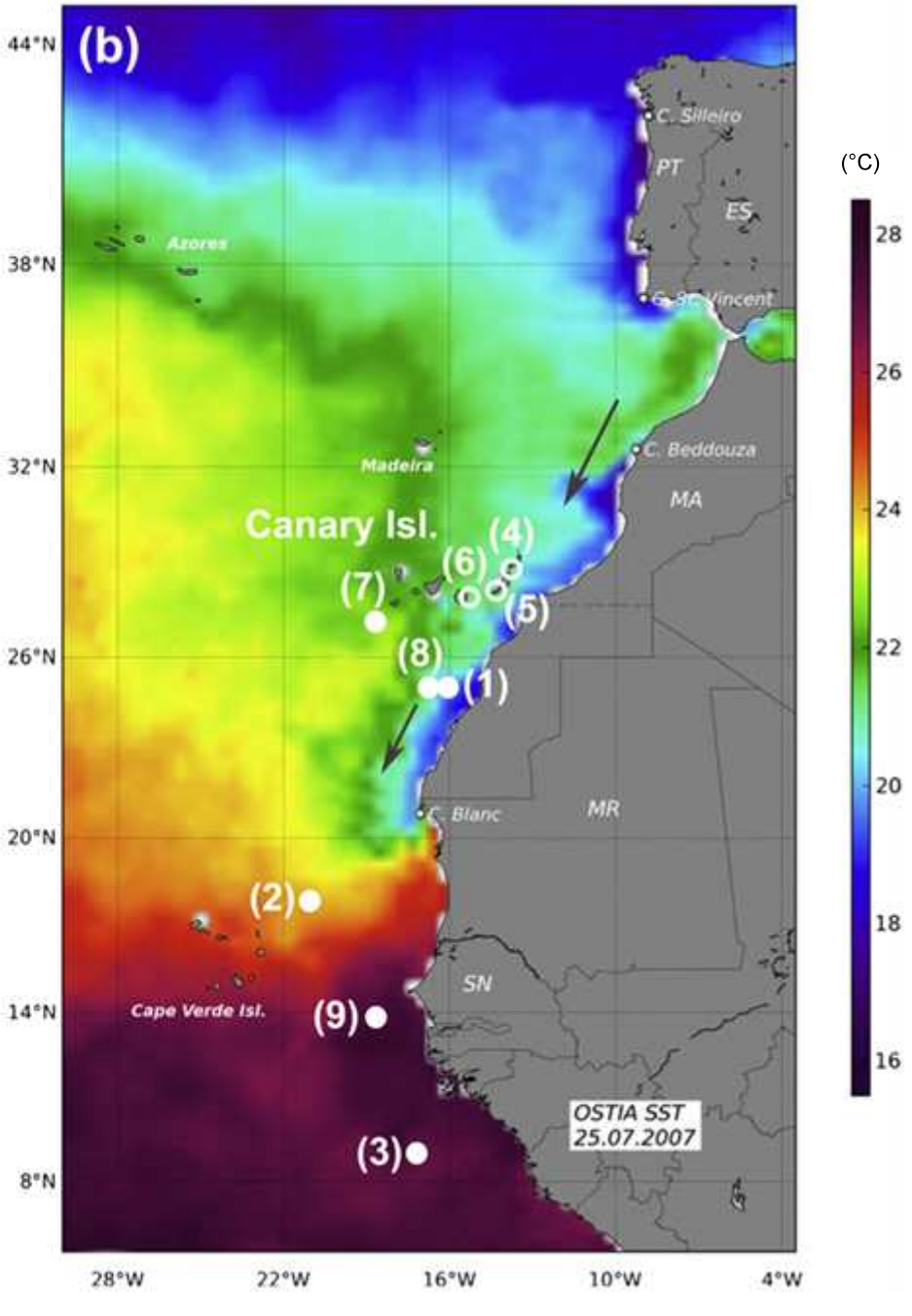

(b)

(1) Sicre et al. (2000)
(2) Matsuzaki et al. (2011)
(3) Castaneda et al. (2009)
(4) This study
(5) Montesinos et al. (2014)
(6) Muhs et al. (2014)
(7), (8), (9) in Hoffman et al. (2017)

(7) GIK15637-1,
(8) M12392-1,
(9) V22-196,


a


b


c


d


e


f

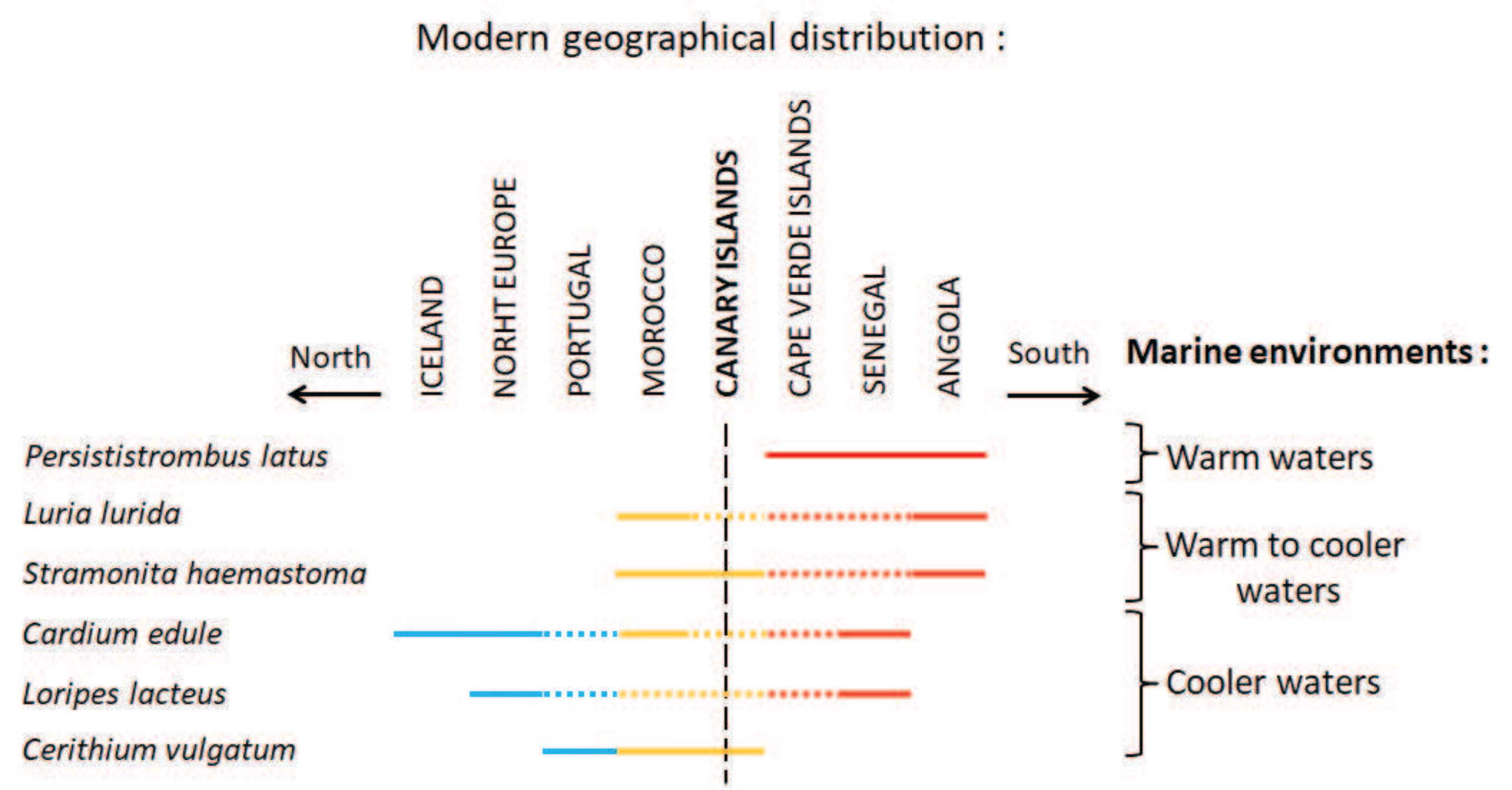
Modern geographical distribution :
North
ICELAND
NORHT EUROPE
PORTUGAL
MOROCCO
CANARY ISLANDS
CAPE VERDE ISLANDS
SENEGAL
ANGOLA
South
Marine environments :
Persististrombus latus
Luria lurida
Stramonita haemastoma
Cardium edule
Loripes lacteus
Cerithium vulgatum
Warm waters
Warm to cooler waters
Cooler waters

(a)
Canary Island sediments

Marine deposits
Paleosols

0 10 20 30

(b)

°C
5
0
-5
-10
Antarctica temperature change (°C)
MIS2
0 10 20 30

(c)

°C
5
0
-5
-10
MIS5.5
MIS5.4
110 120 130 140

(d)

0
-50
-100
-150
Relative sea level (m)
0 10 20 30
Time (ky)

(e)

+6 to +9 m
0
-50
-100
-150
110 116 125 129 140
Time (ky)

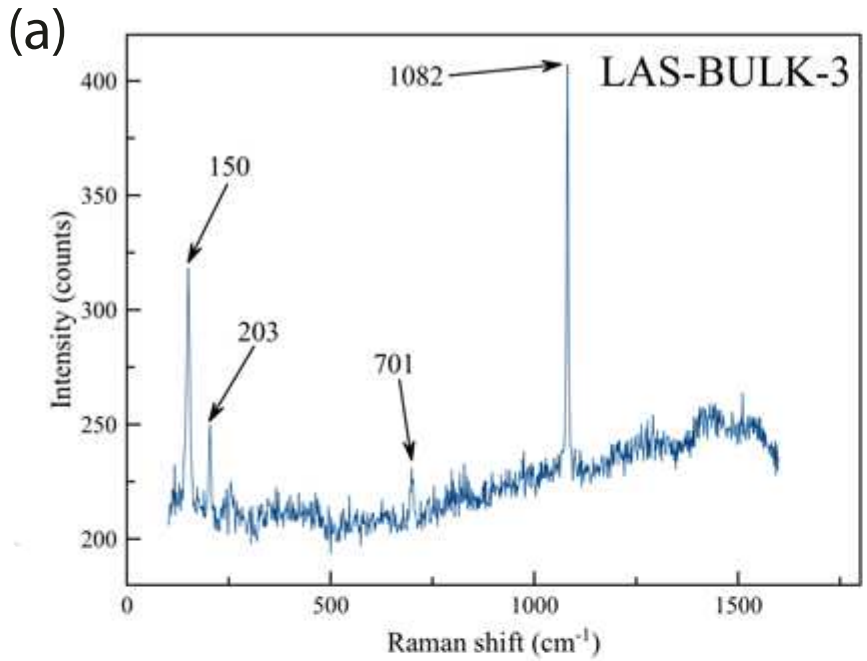
(a)
LAS-BULK-3
1082
150
203
701
Intensity (counts)
Raman shift (cm-1)

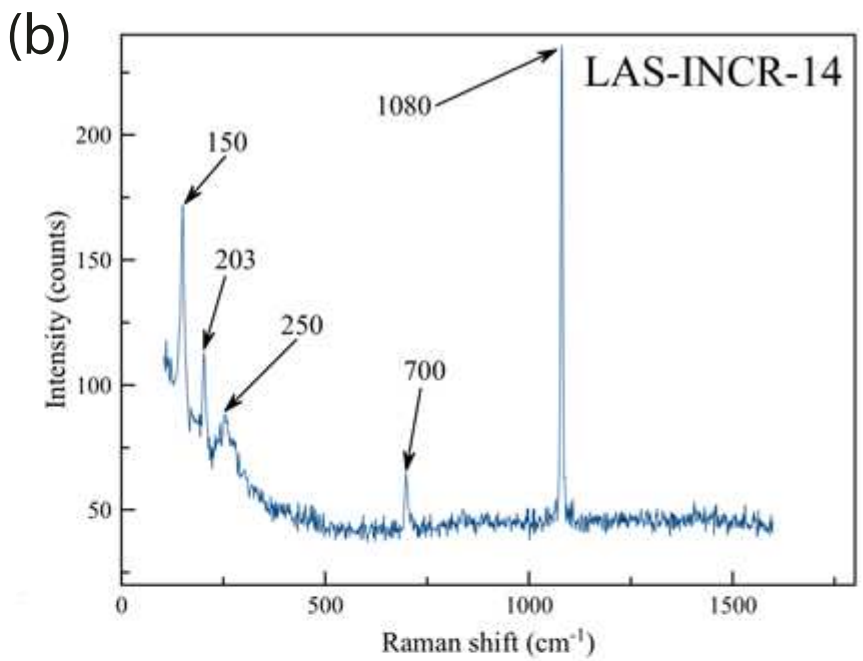
(b)
LAS-INCR-14
1080
150
203
250
700
Intensity (counts)
Raman shift (cm-1)

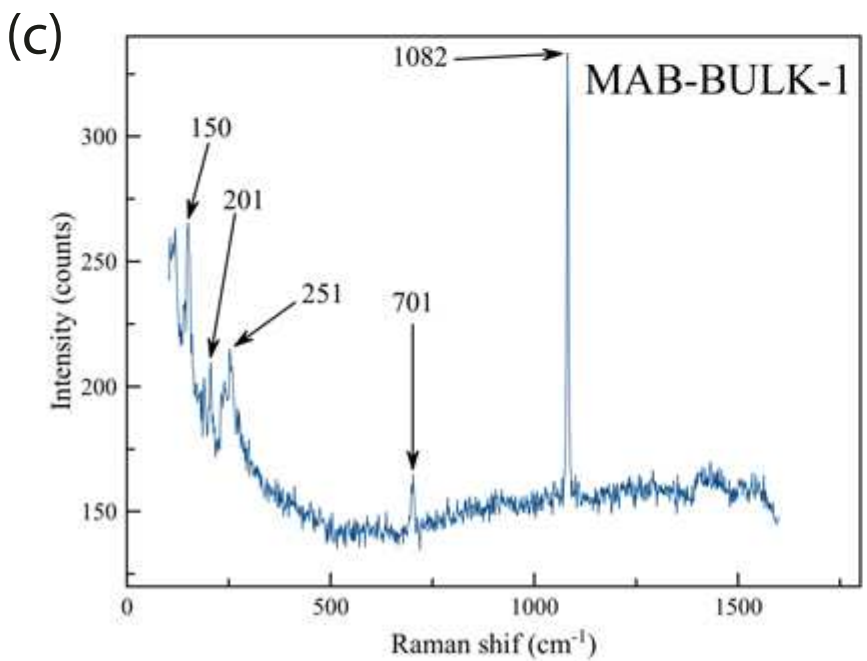
(c)
MAB-BULK-1
1082
150
201
251
701
Intensity (counts)
Raman shif (cm-1)

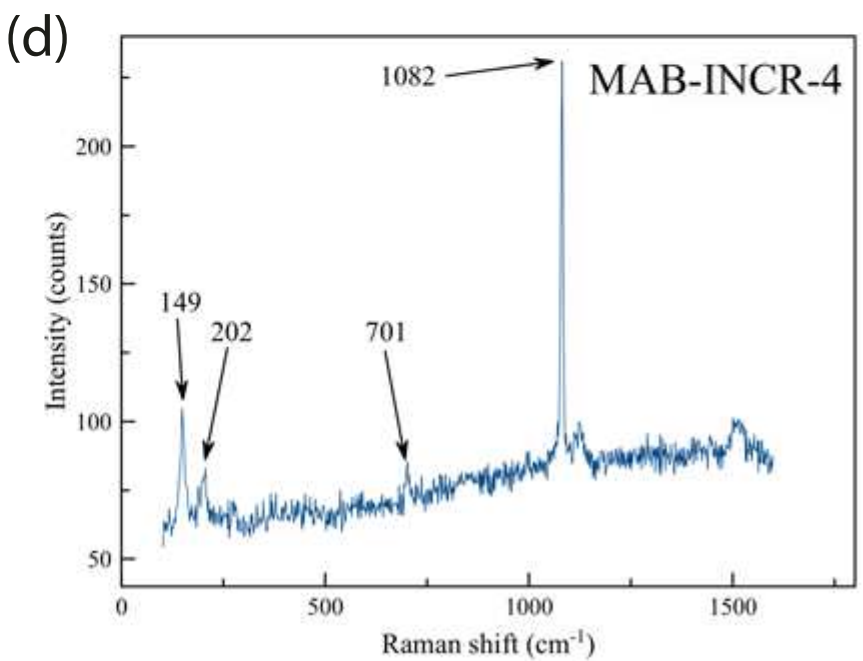
(d)
MAB-INCR-4
1082
149
202
701
Intensity (counts)
Raman shift (cm-1)

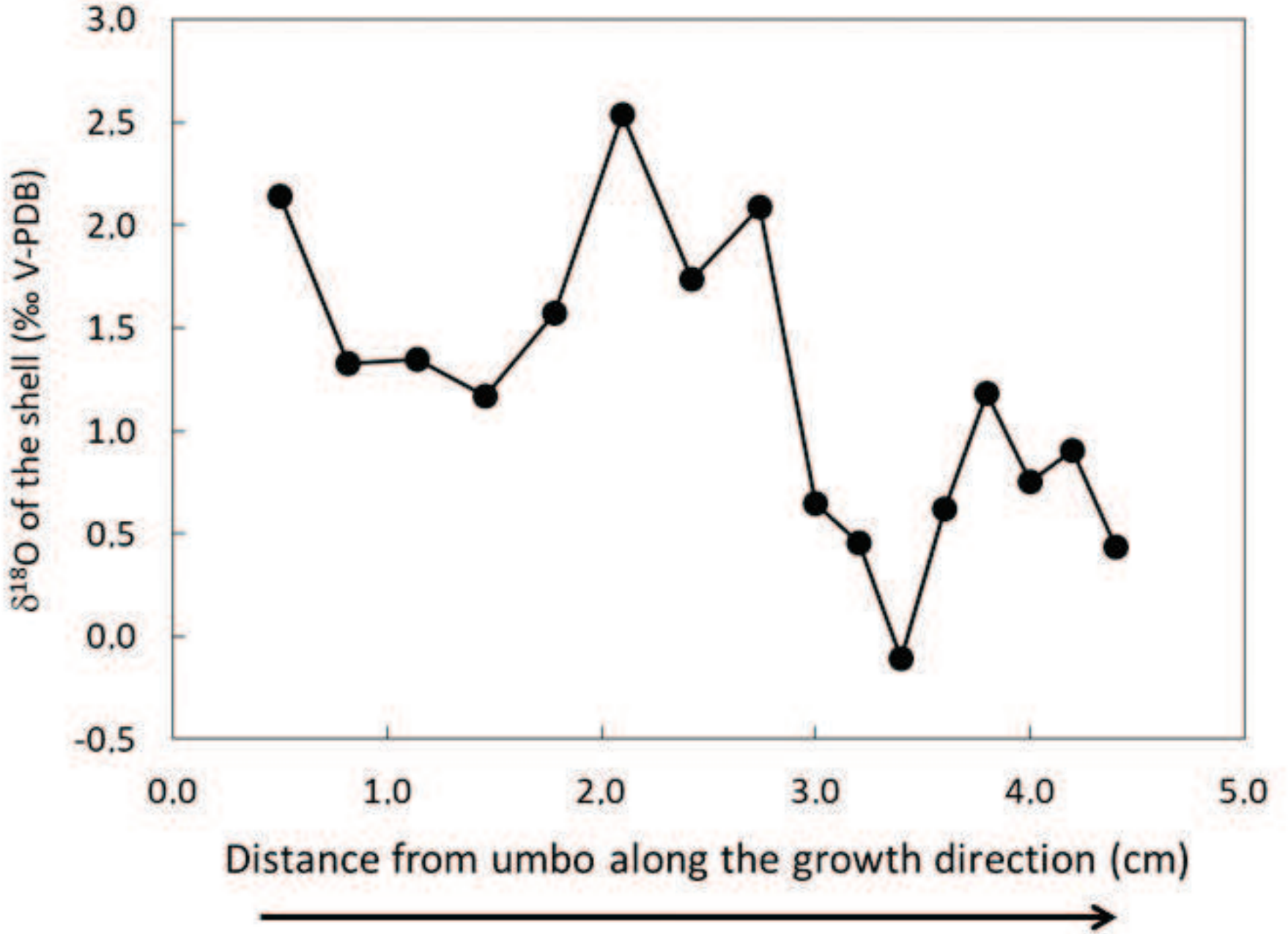
3.0
2.5
2.0
1.5
1.0
0.5
0.0
-0.5
δ18O of the shell (‰ V-PDB)
0.0
1.0
2.0
3.0
4.0
5.0
Distance from umbo along the growth direction (cm)

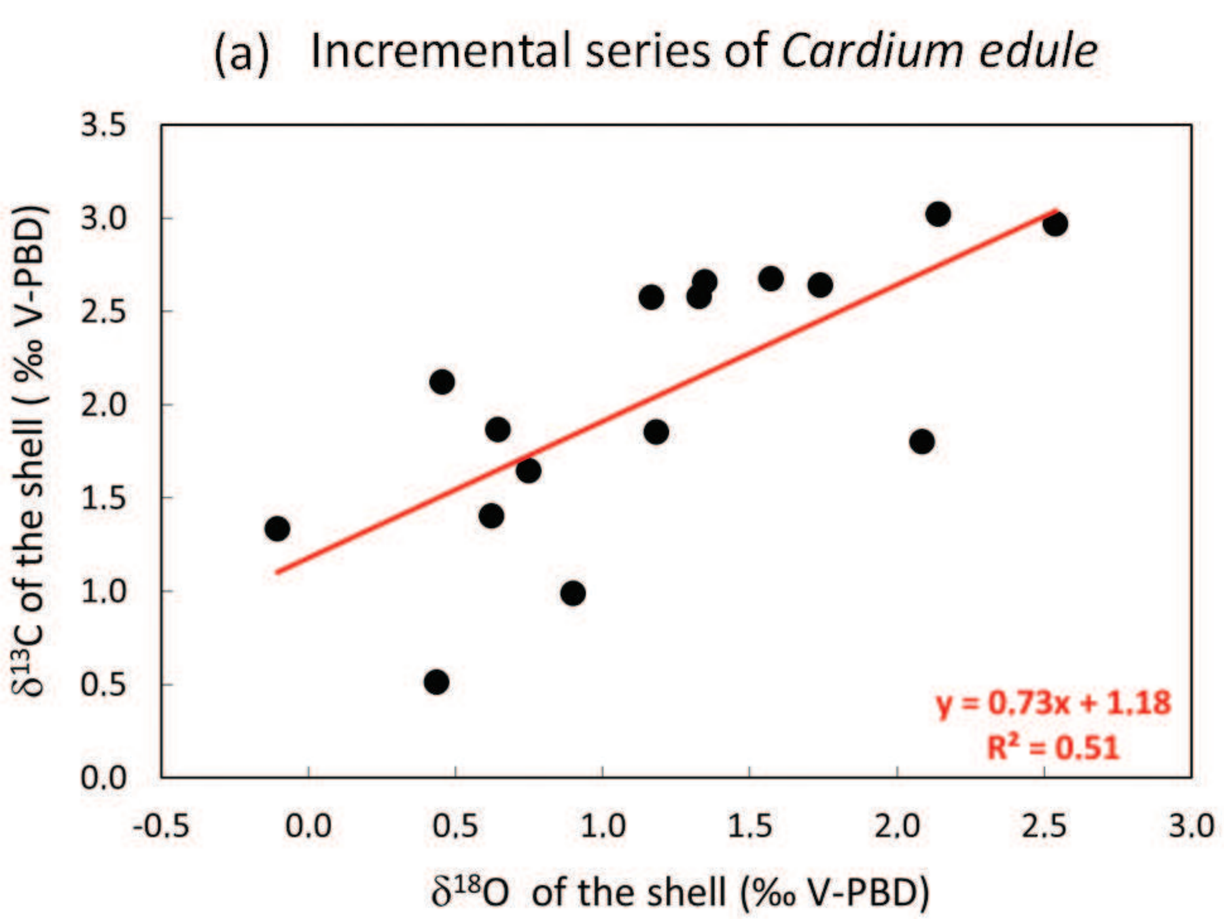
(a) Incremental series of *Cardium edule*
3.5
3.0
2.5
2.0
1.5
1.0
0.5
0.0
δ13C of the shell (‰ V-PBD)
-0.5
0.0
0.5
1.0
1.5
2.0
2.5
3.0
δ18O of the shell (‰ V-PBD)
y = 0.73x + 1.18
R² = 0.51

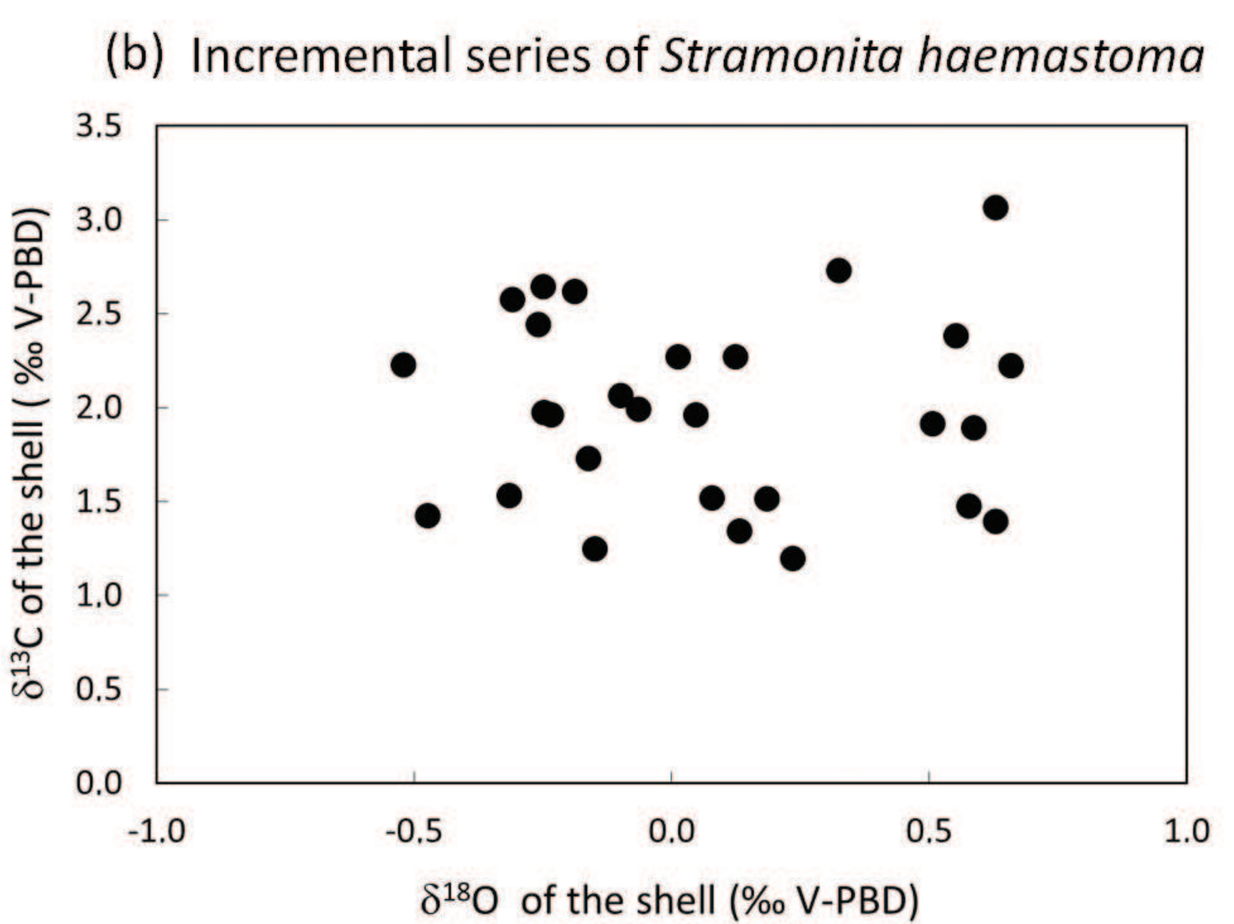
(b) Incremental series of *Stramonita haemastoma*
3.5
3.0
2.5
2.0
1.5
1.0
0.5
0.0
δ13C of the shell (‰ V-PBD)
-1.0
-0.5
0.0
0.5
1.0
δ18O of the shell (‰ V-PBD)

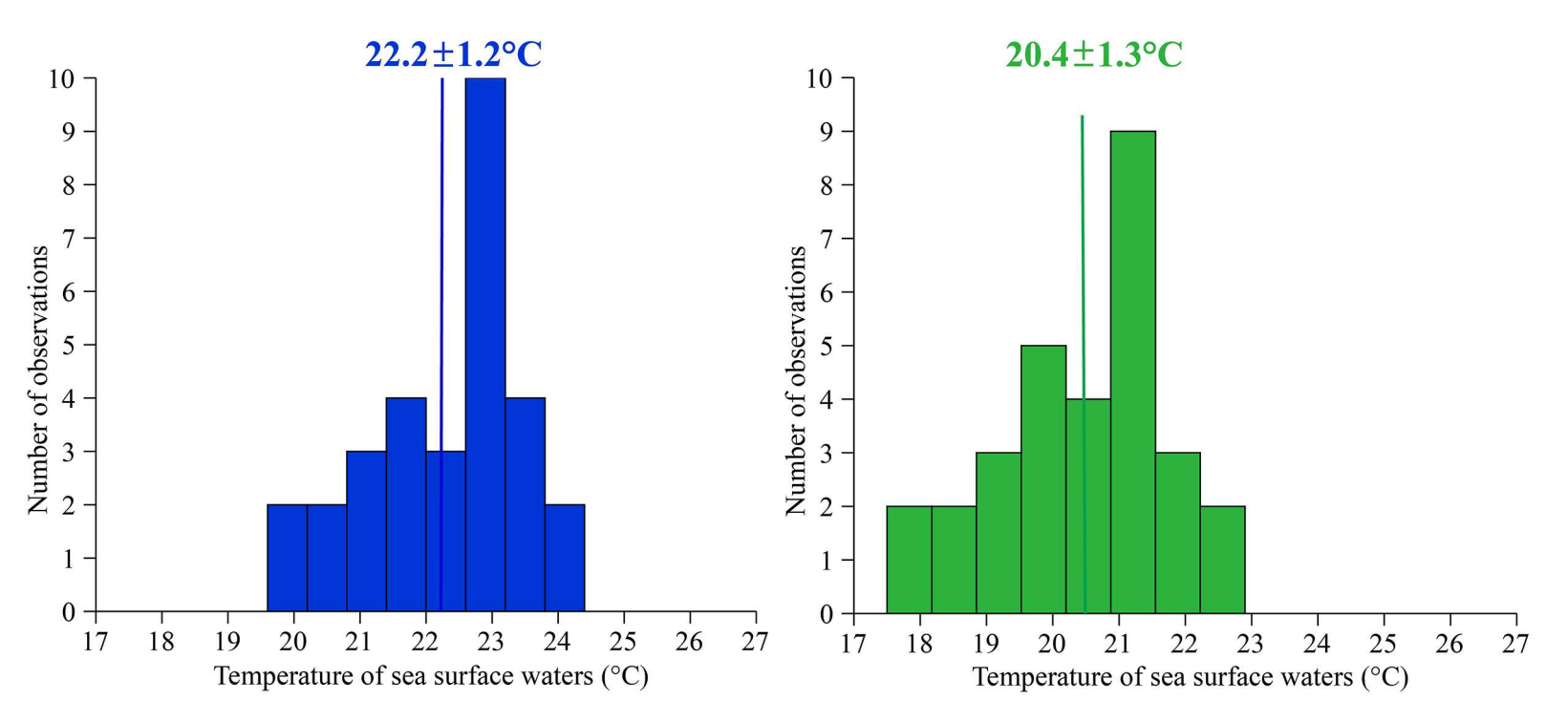
22.2±1.2°C
20.4±1.3°C
Number of observations
Temperature of sea surface waters (°C)
0
1
2
3
4
5
6
7
8
9
10
17
18
19
20
21
22
23
24
25
26
27

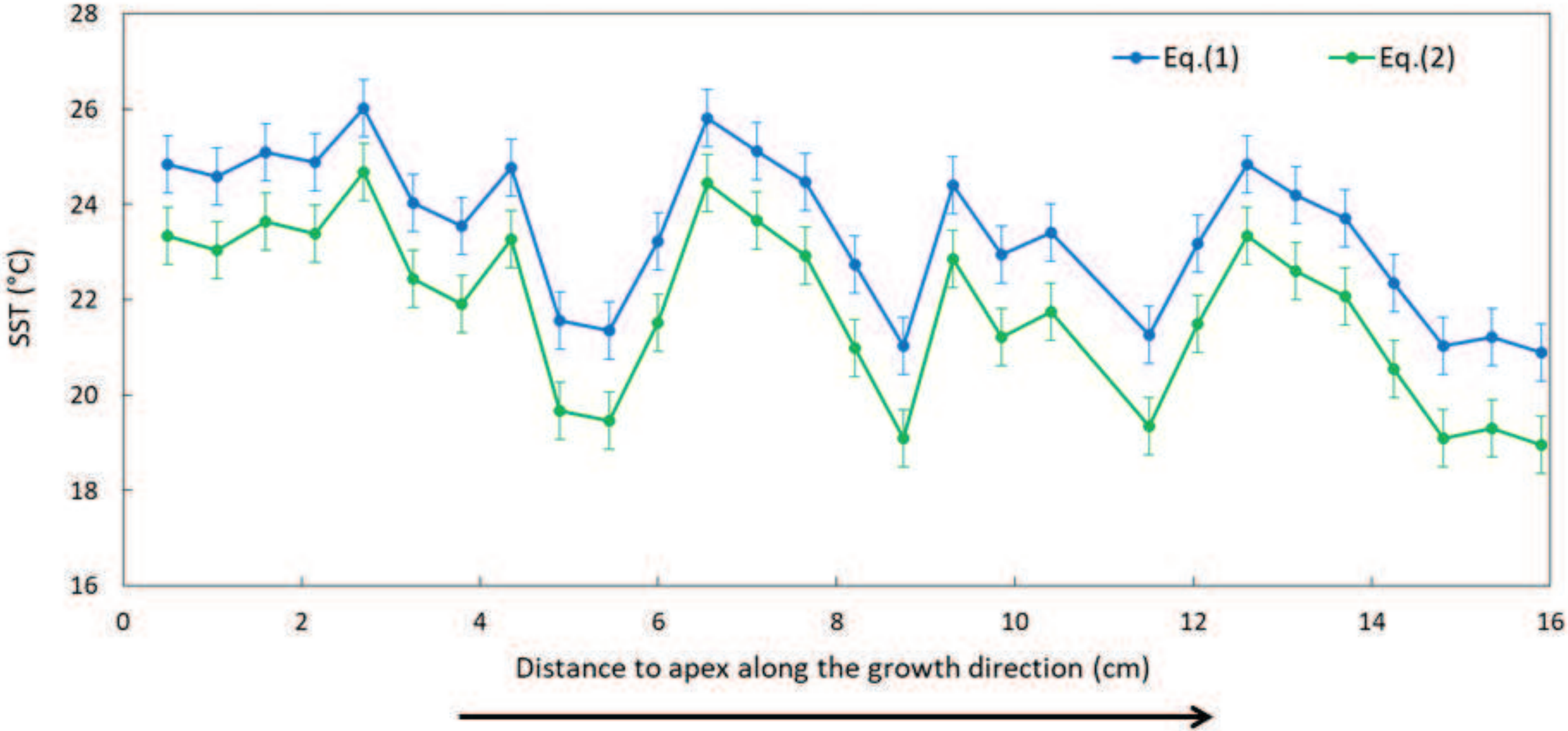
Eq.(1)
Eq.(2)
SST (°C)
28
26
24
22
20
18
16
0
2
4
6
8
10
12
14
16
Distance to apex along the growth direction (cm)

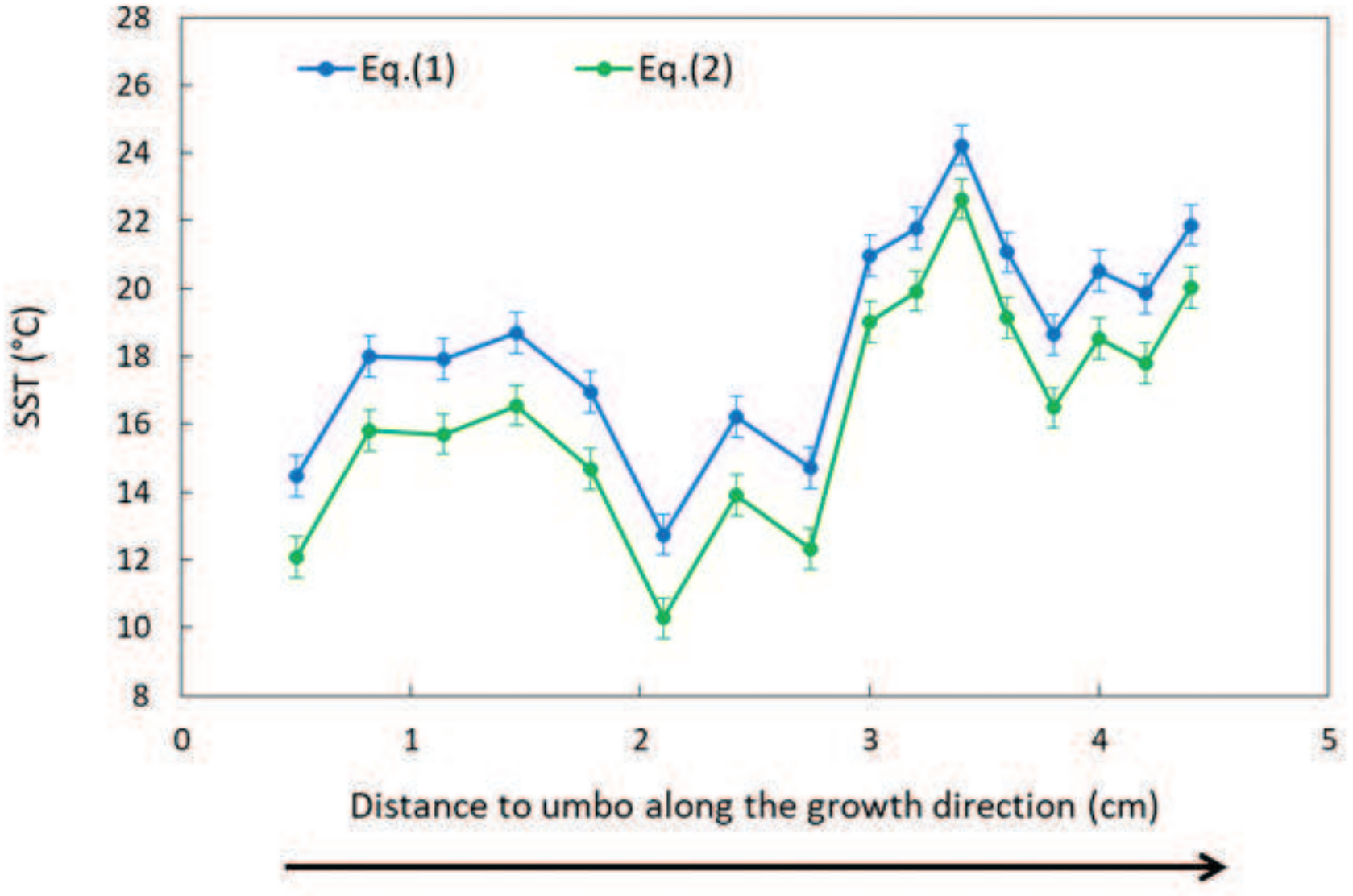
Eq.(1)
Eq.(2)
SST (°C)
28
26
24
22
20
18
16
14
12
10
8
0
1
2
3
4
5
Distance to umbo along the growth direction (cm)

(a) **Relative to core top**

(b) **Relative to the pre-industrial times**

Sea surface temperature anomaly (°C)

+5
+4
+3
+2
+1
0
-1
-2
-3
-4
-5

(1)
(2)
(3)

(1*)
(2*)
(3*)
(4) This study
(5)
(7)
(8)
(9)

120
125
130

110
115
120
125
130

Years (ka BP)

Years (ka BP)

Time

Time

Period	Mean SST (°C)	Method	Authors
2007-2017	20.44°C	Satellite data and *in situ* SST data	Meco et al. (2018)
1993-2014	20.5±0.2°C (*)	Satellite data and *in situ* SST data	Gómez-Letona et al. (2017)
1976-2005	18.5±0.2°C (*)	GCMs simulations	Sousa et al. (2017)
1982-2012	20.3±0.2°C (*)	Satellite data	deCastro et al. (2014)
≤ 2001	≤ 20°C	Atlas 2001	Muhs et al. (2014) from Conkright et al. (2002)
1982-2012	20.3±0.2°C (*)	Satellite data	Santos et al. (2012)

Authors	**Area**	**Proxy or Studies**	**SL anomaly**	**SL highstand(s)**	**Time-period**
Kopp et al. (2013)	47 sites worldwide	Probabilistic analyses on $\delta^{18}O$ of foraminifera	> + 6.6 m	2 highstands separated of +4m	125-116 ky
Spratt and Lisiecki (2016)	sites worldwide	Stack estimates from $\delta^{18}O$ of foraminifera	+6 to + 9m $\pm$12 m		126-119 ky BP
Blanchon et al. (2009)	Yucatan, Mexico	Corals	+ 3 m : + 6m :		126-121 ky 120-117 ky
Thompson et al. (2011)	Bahamas	Corals	+4 m : + 6 m :		$\approx$ 123 ky $\approx$ 119 ky
O'Leary et al. (2013)	Western Australia	Corals	+ 3-4 m : + 9.5 m :		127-119 ky < 118 ky
Dutton et al. (2015b)	Seychelles	Corals	rise : +7.6 m :		129-125 ky < 125 ky
Masson-Delmotte et al. (2013)	–	SL synthesis work	+ 6 m	2 highstands separated of +4m	129-116 ky
Dutton et al. (2015a)	–	SL synthesis work	+ 6 to + 9 m :	Peak :	129-116 ky < 125 ky (122-119 ky)
Capron et al. (2017a,b)	–	LIG studies	+ 6 to + 9 m :	2-phases, late peak :	 122-119 ky

Reference	Material	SST Proxy
Sicre et al. (2000)	Sediment core	$U^{K'}_{37}$
Matsuzaki et al. (2011)	Sediment core	Planktonic foraminiferal assemblages
Castañeda et al. (2009)	Sediment core	$U^{K'}_{37}$
This study	Marine deposits	$\delta^{18}O$ from mollusk shells
Montesinos et al. (2014)	Marine deposits	Extralimital species
Muhs et al. (2014)	Marine deposits	Extralimital species
Hoffman et al. (2017)	Sediment cores	Planktonic foraminiferal assemblages